

Article

Double High-Level Ozone and PM_{2.5} Co-Pollution Episodes in Shanghai, China: Pollution Characteristics and Significant Role of Daytime HONO

Kejing Yang ¹, Lingdong Kong ^{1,2,*}, Songying Tong ¹, Jiandong Shen ³, Lu Chen ¹, Shengyan Jin ¹, Chao Wang ¹, Fei Sha ⁴ and Lin Wang ¹

- ¹ Shanghai Key Laboratory of Atmospheric Particle Pollution and Prevention, Department of Environmental Science & Engineering, Jiangwan Campus, Fudan University, Shanghai 200438, China; 17210740017@fudan.edu.cn (K.Y.); ldkong@fudan.edu.cn (L.K.); 17210740012@fudan.edu.cn (S.T.); 18210740037@fudan.edu.cn (L.C.); 19210740019@fudan.edu.cn (S.J.); 19210740057@fudan.edu.cn (C.W.); lin_wang@fudan.edu.cn (L.W.)
- ² Institute of Eco-Chongming, East China Normal University, No. 3663 Northern Zhongshan Road, Shanghai 200062, China
- ³ Hangzhou Environmental Monitoring Center, Hangzhou 310007, China; 052047010@fudan.edu.cn
- ⁴ Pudong New Area Environmental Monitoring Station, No. 51 Lingshan Road, Shanghai 200135, China; pdsf@sina.com
- * Correspondence: ldkong@fudan.edu.cn



Citation: Yang, K.; Kong, L.; Tong, S.; Shen, J.; Chen, L.; Jin, S.; Wang, C.; Sha, F.; Wang, L. Double High-Level Ozone and PM_{2.5} Co-Pollution Episodes in Shanghai, China: Pollution Characteristics and Significant Role of Daytime HONO. *Atmosphere* **2021**, *12*, 557. <https://doi.org/10.3390/atmos12050557>

Academic Editors: Makiko Nakata and Mizuo Kajino

Received: 15 March 2021

Accepted: 23 April 2021

Published: 26 April 2021

Publisher's Note: MDPI stays neutral with regard to jurisdictional claims in published maps and institutional affiliations.



Copyright: © 2021 by the authors. Licensee MDPI, Basel, Switzerland. This article is an open access article distributed under the terms and conditions of the Creative Commons Attribution (CC BY) license (<https://creativecommons.org/licenses/by/4.0/>).

Abstract: In recent years, high fine particulate (PM_{2.5}) pollution episodes with high ozone (O₃) levels have been observed in Shanghai from time to time. However, their occurrence and characteristics remain poorly understood. Meanwhile, as a major precursor of tropospheric hydroxyl radical (OH) that initiates the formation of hydroperoxyl and organic peroxy radicals, HONO would inevitably affect the formation of O₃, but its role in the formation of O₃ during the double high-level PM_{2.5} and O₃ pollution episodes remains unclear. In this study, the characteristics of the double high pollution episodes and the role of HONO in O₃ formation in these episodes were investigated based on field observation in urban Shanghai from 2014 to 2016. Results showed that high PM_{2.5} pollution and high O₃ pollution could occur simultaneously. The cases with data of double high O₃ and PM_{2.5} concentrations accounted for about 1.0% of the whole sampling period. During the double high pollution episodes, there still existed active photochemical processes, while the active photochemical processes at high PM_{2.5} concentration were conducive to the production and accumulation of O₃ under a VOC-limited regime and a calm atmospheric condition including high temperature, moderately high relative humidity, and low wind speed, which in turn enhanced the conversions of SO₂ and NO₂ and the formation and accumulation of secondary sulfate and nitrate aerosols and further promoted the increase of PM_{2.5} concentration and the deterioration of air pollution. Further analysis indicated that the daytime HONO concentration could be strongly negatively correlated with O₃ concentration in most of the double high pollution episodes, revealing the dominant role of HONO in O₃ formation during these pollution episodes. This study provides important field measurement-based evidence for understanding the significant contribution of daytime HONO to O₃ formation, and helps to clarify the formation and coexistence mechanisms of the double high-level O₃ and PM_{2.5} pollution episodes.

Keywords: O₃; PM_{2.5}; HONO; double high pollution; secondary aerosol

1. Introduction

Shanghai is located in the eastern coast of the Yangtze River Delta (YRD), adjacent to the East Sea. As one of the largest metropolises in China, Shanghai has undergone rapid growth in economic and industrial development and urbanization over the past few decades. The increasing population density and world level industry concentrations

have led to escalating energy consumption and large emissions of pollutants [1], which substantially resulted in severe regional air pollution [2–5]. O₃ and PM_{2.5} (particles with aerodynamic diameter ≤2.5 μm) are the two most important pollutants in major Chinese city clusters such as YRD and have drawn increasing attention due to their impacts on visibility [6], human health [7], and climate change [8].

Previous studies have reported that the secondary aerosols, including secondary inorganic aerosols (SIA: SO₄²⁻, NO₃⁻, and NH₄⁺) and secondary organic aerosols (SOA), are the main contributors to fine particulate in China. For example, SIA account for about 50% of PM_{2.5} mass concentrations [9]. Due to complex photochemical reactions among primary pollutants such as SO₂, NO_x, and volatile organic compounds (VOCs) in the presence of solar radiation, a large number of SIA and SOA are generated, which constitute the main components of PM_{2.5} and increase its concentration. As a secondary pollutant, O₃ in the troposphere is mainly produced by photochemical reactions, and NO_x and VOCs generated from motor vehicles and industrial emissions are the main precursors of O₃ formation [10]. Generally, in the troposphere, NO₂ photolysis at λ < 420 nm generates NO and atomic oxygen O (³P), then the formed O (³P) interacts with O₂ to produce O₃. Once formed, O₃ readily reacts with the formed NO to regenerate NO₂, resulting in a null cycle when no other chemical oxidant species were involved. However, in the troposphere, there exist alternative oxidants (e.g., HO₂ and RO₂) that efficiently convert NO to NO₂, which results in the accumulation of O₃ [10], and therefore, NO₂ photolysis initiates the principal O₃-forming reaction in polluted air. Strong solar radiation, high temperature, and low wind speed are beneficial to the formation and accumulation of O₃ [10–13].

Some studies have been performed to investigate particulate matter pollution and/or O₃ pollution [13–16]. The concentration of PM_{2.5} presents a distinct seasonal variation, generally showing high values in winter and low ones in summer [17–19]. High particulate matter pollution often corresponds to low concentrations of O₃ in cold seasons [20], and low airborne particulates to high O₃ pollution in warm seasons [21]. However, several studies have shown that some air pollution events present high levels of O₃ and particulates concurrently worldwide in recent years. For example, Awang et al. reported that ground-level O₃ concentrations were higher during high particulate events (HPE) than those during non-HPE in Malaysia [22]. Ding et al. found that biomass burning in agricultural activities caused high PM_{2.5} and O₃ pollution in Nanjing, eastern YRD [17]. Tie et al. found the co-occurrence of high PM_{2.5} and O₃ concentrations during late spring and early fall in eastern China [23]. Wang et al. investigated the primary characteristic of the high co-occurring concentrations of O₃ and PM_{2.5} in YRD in the summer of 2013 [24]. However, the research on the double high-level O₃ and PM_{2.5} pollution in the YRD and the corresponding occurrence mechanism is still very limited.

In addition, the surface O₃ concentration in China is increasing year by year [25], which is often considered to be closely related to the decrease in PM_{2.5} concentration. This is because that the light extinction of aerosols weakens O₃ photochemistry, resulting in a significant reduction in the net chemical production of O₃, and therefore the increase of surface O₃ concentration in China was usually attributed to the high concentrations of O₃ aloft being entrained by turbulence from the top of the planetary boundary layer to the surface [26]. However, high particulate pollution episodes with high O₃ levels are observed from time to time in China. Furthermore, nitrous acid (HONO) has been recognized as a major precursor of tropospheric OH radical that initiates daytime atmospheric photochemistry [27,28]. For example, Kim et al. reported that HONO photolysis was the dominant OH source, contributing 80.4% of atmospheric primary OH production in the wintertime in Weld Country, Colorado [27]. A recent modelling study found that HONO photolysis acted as the dominant source for primary OH production with a contribution of more than 92% based on a winter field campaign conducted at a rural site of the North China Plain [28]. The primary OH production from the HONO photolysis enhances the formation of hydroperoxyl and organic peroxy radicals, and hence affects the formation of O₃. Some modeling studies showed that elevated levels of HONO considerably enhanced the ROx

(= OH + HO₂ + RO₂) concentrations and accelerated the RO_x cycles across the Jing-Jin-Ji and coastal regions of China [29,30], and HONO photolysis during the daytime could significantly enhance O₃ formation in the polluted boundary layer [23,31,32]. However, up to now, few studies have been reported on the impact of HONO on O₃ formation during the specific double high-level PM_{2.5} and O₃ pollution episodes.

In this study, based on a continuous field observation from 2014 to 2016 in Shanghai, a comprehensive analysis was carried out to investigate the characteristics and the formation and coexistence mechanisms of the double high-level PM_{2.5} and O₃ pollution episodes. Meanwhile, the impact of daytime HONO on O₃ formation during the double high pollution episodes was also investigated. This study will help to further understand the characteristics and occurrence mechanism of the double high pollution episodes and the role of daytime HONO in O₃ formation in these pollution episodes.

2. Materials and Methods

2.1. Sampling Site Description

In this study, sampling was conducted from 3 April 2014, to 31 December 2016, in Pudong New Area Environmental Monitoring Station in Shanghai, China (31.23° N, 121.53° E) (Figure 1). Shanghai is one of the largest cities in the YRD region, and this site is representative of urban areas due to the high traffic density and residential and industrial emissions. Climatically, Shanghai has a subtropical monsoon climate, with four distinct seasons, that is, spring (March, April, and May), summer (June, July, and August), autumn (September, October, and November), and winter (December, January, and February). The annual average temperature (T), relative humidity (RH), and rainfall are about 16.3 °C, 78.4%, and 1182.8 mm, respectively.



Figure 1. Map of the geographical location of the observation site.

2.2. Water-Soluble Inorganic Ion and Trace Gas Measurements

In this study, we acquired hourly mass concentrations of major water-soluble inorganic ions in PM_{2.5} (NH₄⁺, Na⁺, K⁺, Ca²⁺, Mg²⁺, SO₄²⁻, NO₃⁻, and Cl⁻) and trace gases (HCl, HONO, SO₂, HNO₃, and NH₃) by using a continuously on-line Monitor for Aerosols and Gases in Ambient Air (MARGA, ADI 2080, Applikon Analytical B.B Corp., Netherlands) with a Teflon-coated PM_{2.5} cyclone inlet. The detailed information about the MARGA instrument was given in previous studies [33,34]. Briefly, the instrument consists of a sampling box and an analytical box. The sampling box is comprised of a wet rotating denuder (WRD) for trace gas absorbing and a steam jet aerosol collector (SJAC) for particle collecting. The ambient air sampling for MARGA was performed at a flow rate of 1 m³/h through the inlet by using a pump equipped with a mass flow controller. Gaseous species

were absorbed and dissolved into the liquid coated inter surface of the WRD, and then particles in the stream passed through the WRD and arrived in the SJAC to be condensed into droplets rapidly. After collecting for every hour, the two collected liquid samples were analyzed by ion chromatography with a C4 100 × 4 mm column for cations and a supp. 10–75 column for anions. MARGA was automatically calibrated by an internal calibration method using a lithium bromide solution. MARGA was also routinely calibrated by using a mixed cation and anion external standard solution in a routine time to ensure data quality.

2.3. $PM_{2.5}$ Mass Concentrations and Trace Gases

Hourly mass concentration of $PM_{2.5}$ and trace gas species, including SO_2 , O_3 , and NO_x , were continuously measured using a tapered element oscillating microbalance (TEOM 1405-D, Thermo Scientific Co., Waltham, MA, USA) and a series of gas analyzers (Ecotech EC9850B SO_2 automatic monitor for SO_2 , 49i, and 42i gas analyzers for O_3 and NO_x , respectively, Thermo Scientific, USA). The high-resolution data during the sampling time were converted to hourly means. The analytical instruments were also routinely calibrated by using external standard gases, including daily zero check and weekly span calibrations to ensure data quality. It is worth noting that the TEOM measured mass has a strong temperature and RH dependence, and the effect is larger at larger concentrations, which leads to mass underestimation. Loss of semi-volatile compounds is the probable cause [35,36]. Therefore, the TEOM method underestimates $PM_{2.5}$ mass, and the underestimation is greater at high concentrations [35,36], which may mean that the actual $PM_{2.5}$ pollution in the double high pollution cases may be more serious than that revealed by the measured $PM_{2.5}$ mass data.

2.4. Meteorological Data

The hourly meteorological parameters, including T, RH, wind speed (WS), wind direction (WD), visibility (Vis), and precipitation, were obtained from the same environmental monitoring station. Meteorological datasets, including global solar radiation (SR) and boundary layer height (BLH), were derived from ADS (<https://ads.atmosphere.copernicus.eu/cdsapp#!/home>) (accessed on 9 August 2020) and ECMWF ERA-Interim reanalysis (<https://apps.ecmwf.int/datasets/data/interim-full-daily/levtype=sfc/>) (accessed on 10 August 2020) in a $0.125^\circ \times 0.125^\circ$ grid, respectively.

3. Results and Discussion

3.1. Overview of $PM_{2.5}$ and Trace Gas Pollution in Shanghai

3.1.1. Seasonal Behaviors

Figure 2 shows the monthly variations of $PM_{2.5}$, O_3 , NO, NO_x , CO, and SO_2 in Shanghai during the period of April 2014–December 2016. As can be seen from Figure 2a, O_3 exhibits a distinguished seasonal variation during the observation period. In 2014, the curve of monthly O_3 concentration shows a sharp peak in late spring and a broad one in early autumn (a maximum in May and a secondary maximum in September). In 2015, O_3 concentration increased from January on and reached a relatively high level in May, which is a secondary maximum value of the whole year. Then, after a slight drop in June, it continued to increase until it reached a maximum value in September. The O_3 variation trend in 2016 is similar to that in 2014, while a slightly increasing trend appears in July rather than a drop in the same month of 2014. The observed seasonal characteristics from 2014 to 2016 in Shanghai are different from previous studies conducted in southern and northern China. For example, a summer minimum and an autumn maximum of O_3 were reported in Hong Kong [37], and an early summer (June) broad maximum was found in Beijing [38,39]. However, the seasonal cycle of O_3 concentrations exhibits similar trends as those found at Lin'an site on the southern edge of the YRD [40–42], in which O_3 concentration showed a maximum in May and a sharp drop in July. Shanghai is in the eastern region of YRD and verges on the East Sea, which is on the upwind of the southeast summer monsoon. Therefore, the local emission of Shanghai and the intense solar radiation

could be the main causes of O_3 formation in summer, resulting in a different seasonal cycle of O_3 compared to other inland cities of YRD. In fact, the NO_x and CO (Figure 2c,f) show a relatively high level in summer (about 20 and 500 ppbv, respectively). As mentioned above, it is noticeable that a slight drop of O_3 concentration was found in summer compared to other seasons. Although high temperature and high solar radiation intensity in summer could promote the formation of O_3 , the marine air transported from the Pacific Ocean from time to time due to the subtropical summer monsoon climate of Shanghai will not only increase precipitation (Table S1) but also bring strong winds, leading to a significant reduction of O_3 concentration from June to August. In addition, O_3 concentration shows a low level in winter. This could be attributed to weaker solar radiation, lower temperature, and high level of NO (Figure 2d), because the weaker solar radiation and lower temperature decreased atmospheric photochemical reactivities and the high NO level enhanced the chemical titration of O_3 , and therefore O_3 production was suppressed.

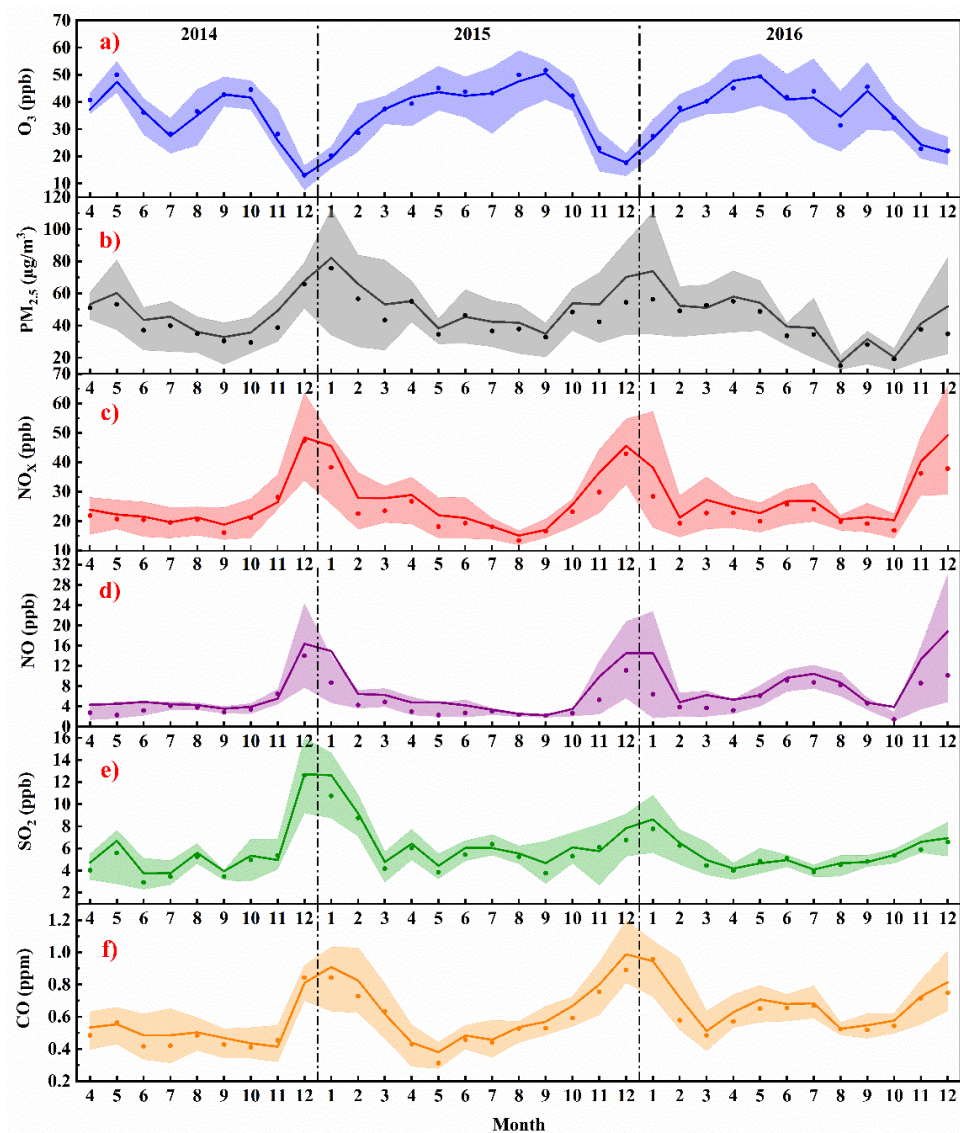


Figure 2. Seasonal variations of (a) O_3 , (b) $PM_{2.5}$, (c) NO_x , (d) NO, (e) SO_2 , and (f) CO. Bold solid lines are the median values, diamonds show the monthly averages, and thin solid lines represent percentiles of 75% and 25%.

Figure 2b gives the month-to-month concentration variations of fine particle $PM_{2.5}$ from 2014 to 2016. It shows an overall well-defined seasonal pattern with the maximum in winter (January) and the minimum in early autumn (September in 2014 and 2015) or late

summer (August in 2016). This distinct seasonal variation could be attributed to more fossil fuel combustion emissions in colder seasons and less in warmer seasons, and the changes of ambient vertical mixing processes and deposition in different seasons. On the one hand, local fossil fuel combustion emissions increased in winter. On the other hand, as we know, the increased fossil fuel combustion emissions during the winter heating period in the North China Plain enhanced the particulate matter and other trace gases concentrations of YRD region via long-range transport [15,43]. Atmospheric conditions such as lower mixing layer height and lower temperature would decrease the horizontal and vertical mixing processes. Furthermore, deposition would have a distinguished seasonal variation, because heavy precipitation in summer led to wet-deposition and high soil humidity and the growth of deciduous plants promoted the dry deposition of particulate matter in warmer seasons [44]. The relatively low concentration of $PM_{2.5}$ in summer might be partly due to the increase of mixing boundary layer height and the more active vertical process [19]. It is worth noting that $PM_{2.5}$ concentration showed a strong change in the monthly curve from 2014 to 2016. For instance, an apparent drop in February could be found both in 2015 and 2016, as well as a sudden drop in October 2016. The concentration drops of $PM_{2.5}$ together with other primary pollutants (i.e., SO_2 , CO, NO_x) in February were mainly due to the winter break of the Chinese Spring Festival and the ban on setting off fireworks in Shanghai during the festival. In addition, it can be clearly seen that the month-by-month change patterns of $PM_{2.5}$ from 2014 to 2016 are similar to that of NO_x , indicating that vehicle emissions and fuel combustion emissions have important impacts on $PM_{2.5}$ concentration.

3.1.2. Distinguishment of Double High-Level O_3 and $PM_{2.5}$ Episodes

Figure 3a–c displayed the scatter plots of O_3 - NO_x , CO- NO_x , and $PM_{2.5}$ - O_3 relationships during the whole observation period, respectively. Moreover, to analyze the influence of related factors, the dataset points were color-coded with different parameters such as ambient temperature and O_3 concentration. Figure 3a illustrated the scatter plots of O_3 and NO_x measured at the observation site with temperature during the whole observation period. As reported in previous studies [17,19], O_3 showed an overall negative correlation with NO_x based on the whole dataset. The colored scatters showed that the negative correlation mainly occurred at lower ambient temperature, indicating a titration effect of freshly emitted NO with O_3 in cold seasons and/or an impact of high RH, especially at night. In contrast, a positive correlation between O_3 and NO_x was found at higher temperatures (>25 °C) and a moderate level of NO_x concentration (<100 ppbv), which mainly occurred in the daytime of warmer seasons. This result possibly suggested an intensely active photochemical reaction of O_3 production in summer, which led to a strong seasonal variation pattern, as shown in Figure 2a. In addition, it is worth noting that there is usually a negative correlation between T and RH, and O_3 can react with water vapor to some extent or dissolve in particles containing liquid water, which would also cause low O_3 concentration at low T and high RH. In other words, low T and high RH are not conducive to the formation and accumulation of O_3 .

Generally, CO has a good correlation with VOCs and plays a similar role as VOCs in photochemical O_3 production [12], and thus in this study CO was chosen as the reference species for VOCs, because VOCs were not measured. A scatter plot of CO and NO_x color-coded with O_3 concentration was provided by Figure 3b. It is found that high concentration of O_3 was usually associated with high CO/ NO_x ratio, and an increase of CO always led to higher O_3 concentration when NO_x concentration was lower than 75 ppbv, while NO_x reversed. This relationship based on CO- O_3 - NO_x suggested a VOC-limited regime of O_3 formation in urban Shanghai. The inset in Figure 3b also specifically illustrated the VOC-limited region of our observation site. This result is similar to the previous studies by Ding et al. and Chen et al., who also found a VOC-limited regime in urban sites of Nanjing and Hangzhou in YRD, respectively [2,17].

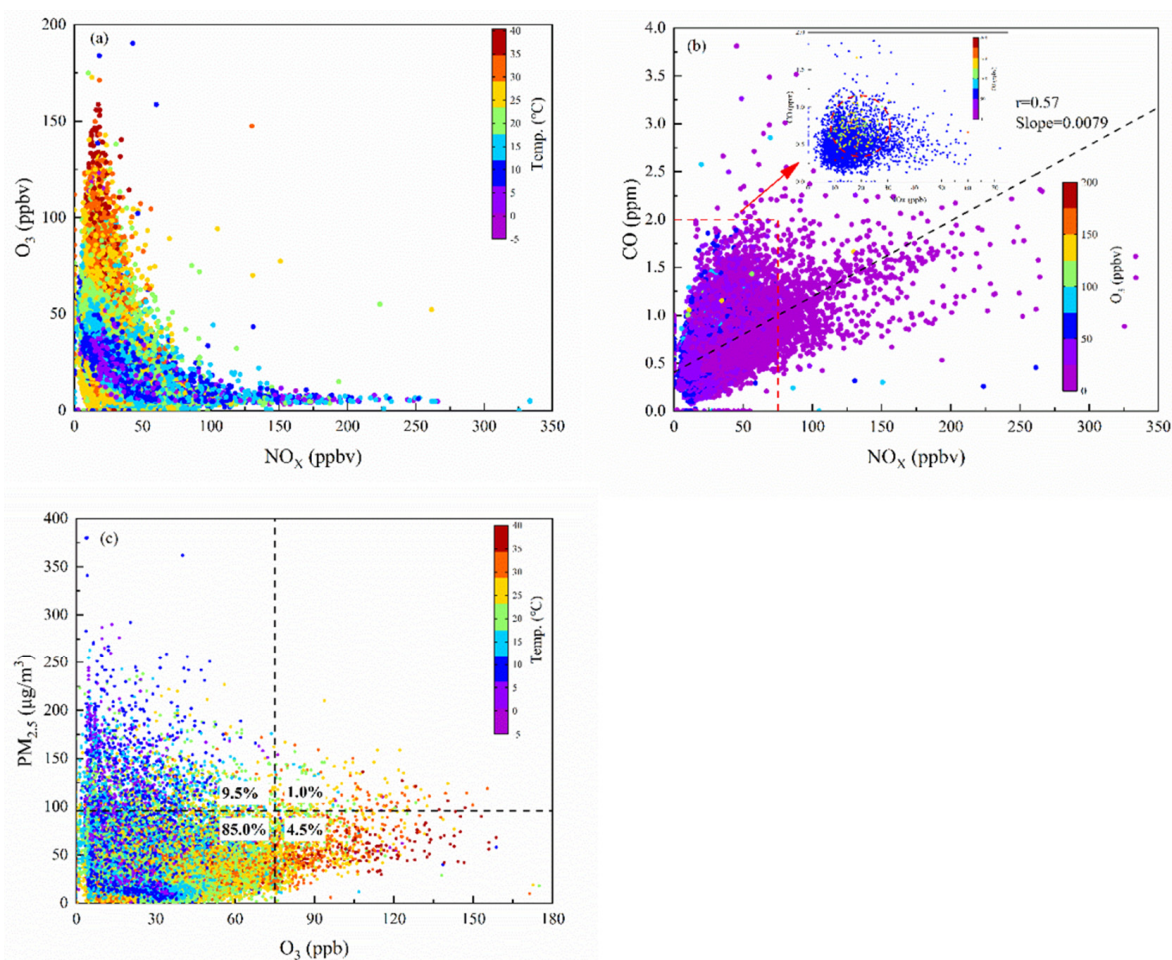


Figure 3. Scatter plots of selected parameters during the whole observation period. (a) O_3 - NO_x color-coded with air temperature, (b) CO - NO_x color-coded with O_3 , and (c) $PM_{2.5}$ - O_3 color-coded with air temperature.

The color-coded scatter plots in Figure 3c showed overall high O_3 concentrations at high temperature and high $PM_{2.5}$ levels at the reverse situation. The relationship of $PM_{2.5}$ and O_3 indicated a significantly positive correlation under higher temperature and a negative correlation under low ambient temperature. Similar results were found in Nanjing and Hangzhou by previous reports [2,17,19]. The positive correlation suggested that a high concentration of O_3 was favorable to the formation of secondary aerosols in $PM_{2.5}$ at high temperatures. The anti-correlation for cold air might be mainly attributed to the strong titration effect of NO in cold seasons and the dimming effect of high $PM_{2.5}$ mass concentration. On the one hand, the increasing slope under high ambient temperatures probably reflected the enhanced formation of secondary particulates, which were closely related to the high conversion rate of SO_2 to sulfate in the presence of high-level O_3 and high solar radiation [45]. Therefore, it led to the mixed pollution of high levels of fine particulate and O_3 in warmer periods. In China, particulate pollution events were often defined as $PM_{2.5}$ daily average concentration exceeded the class-II of the Chinese National Ambient Air Quality Standard (GB3095–2012, $75 \mu\text{g}/\text{m}^3$) [46]. Some studies also defined a specific value as high particulate event according to the actual situation. For instance, Huang et al. suggested that days with PM_{10} levels exceeding $56 \mu\text{g}/\text{m}^3$ were defined as high PM days [47]. On the other hand, previous studies often defined O_3 pollution based on the Chinese National Ambient Air Quality Standard (GB3095–2012), which suggested the limited value of the second grade daily maximum hourly concentration ($200 \mu\text{g}/\text{m}^3$, 93 ppb) and daily hourly concentration ($160 \mu\text{g}/\text{m}^3$, 75 ppb). In this study, the scatter points herein were divided into four regions with the species concentrations of $96 \mu\text{g}/\text{m}^3$ and 75 ppb for $PM_{2.5}$ and O_3 , respectively (marked with black-dotted line). The data with

moderate concentration levels for both PM_{2.5} and O₃ at relatively lower temperatures during the entire three years accounted for about 85.0% of total sampling data points, which indicated that the double low O₃ and PM_{2.5} concentrations mainly occurred in the seasons with moderate temperature. The data with high-PM_{2.5}-low-O₃ concentration at low temperature and the high-O₃-low-PM_{2.5} concentration at high temperature accounted for the second and third proportions (9.5% and 4.5%, respectively) during the whole period. The last but most noticeable was the cases with data of double high O₃ and PM_{2.5} concentrations, accounting for about 1.0% of total sampling data points. It should be pointed out that this pollution mainly occurred between April and September in Shanghai, but it did not easily occur in early spring, late autumn, or winter in Shanghai. The need for active photochemical processes may be an important reason for the occurrence of this pollution, even in the presence of high concentrations of PM_{2.5}.

3.1.3. Characteristics of Double Low-Level O₃ and PM_{2.5} Periods

In the four regions in Figure 3c, double low-level O₃ and PM_{2.5} episodes frequently occurred during the entire observation period (Figure 2a,b). Herein, three typical cases with double low-level O₃ and PM_{2.5} were selected for analysis and comparison, and the corresponding meteorological factors and chemical species concentrations were summarized in Table S2. The three cases occurred from November 26 to November 27, 2014 (denoted as Case 1), from 8 February to 10 February 2015 (denoted as Case 2), and from 12 February to 22 February 2016 (denoted as Case 3), during the three-year observation period, respectively.

In the three cases, the average concentration of PM_{2.5} was $43.5 \pm 25.4 \mu\text{g}/\text{m}^3$, exceeding the first grade of the Chinese National Ambient Air Quality Standard for daily averaged PM_{2.5} concentration (GB3095–2012, $35 \mu\text{g}/\text{m}^3$). The average mass concentrations of PM_{2.5} in Case 2 and Case 3 were 46.9 ± 30.9 and $45.2 \pm 24.3 \mu\text{g}/\text{m}^3$, respectively, and the values were about 1.6 times higher than that of Case 1 ($28.9 \pm 15.6 \mu\text{g}/\text{m}^3$). The PM_{2.5} average mass concentrations in these cases were lower than that in the previous study, which was $66 \pm 29 \mu\text{g}/\text{m}^3$ in non-haze days [5]. The average mass concentration of O₃ was $66.5 \pm 26.8 \mu\text{g}/\text{m}^3$, and it was lower than the second grade of the Chinese ambient air quality standard (GB3095–2012, $160 \mu\text{g}/\text{m}^3$ per hour for O₃ for second grade). The average mass concentrations of SIA and total water-soluble inorganic ions (TWSI) were 26.43 ± 16.70 and $29.13 \pm 17.65 \mu\text{g}/\text{m}^3$, which accounted for 6% and 65% of PM_{2.5}, respectively, and SIA accounted for 89% of the TWSI during double low-level O₃ and PM_{2.5} periods. Both TWSI and SIA during double low-level periods had a good positive correlation with PM_{2.5}, respectively, and their correlation coefficient (r) values with PM_{2.5} were 0.95 and 0.96, respectively, indicating that the TWSI and SIA contributed significantly to PM_{2.5}. The average mass concentrations of NO₃⁻, SO₄²⁻, and NH₄⁺ were 11.97 ± 9.58 , 7.63 ± 4.00 , and $6.83 \pm 4.44 \mu\text{g}/\text{m}^3$ during the double low-level periods, respectively. In the three cases, the average mass concentration of NO₃⁻ obviously exceeded that of SO₄²⁻, indicating high nitrate pollution in Shanghai, which is consistent with the previous studies [48,49]. The occurrence of high nitrate pollution should be attributed to the reduction of SO₂, the increase of NO_x emission due to SO₂ emission control strategies of China, and the rapid increase of NO_x emitted from dramatically increased vehicle population and vigorously developed industries [48,49].

3.2. General Characteristic of Double High-Level O₃ and PM_{2.5} Episodes

In this study, we defined the double high-level O₃ and PM_{2.5} pollution episodes as the condition that PM_{2.5} and O₃ concentrations consecutively exceeded 96 and $160 \mu\text{g}/\text{m}^3$ (75 ppb) for an 8-h period or longer, respectively, and hence a total of nine typical cases were found during the whole field observation period. These mixed pollution cases mainly occurred between April and September in Shanghai, but it did not easily occur in early spring, late autumn, or winter in Shanghai, showing distinct seasonal characteristics. To further understand the pollution characteristics, main cause, and occurrence mechanism of

the mixed pollution episodes with double high-level O₃ and PM_{2.5}, we selected six typical pollution episodes for detailed case studies.

3.2.1. Mixed Pollution Episodes with Double High-Level PM_{2.5} and O₃

Figure 4 and Table 1 described the temporal variations and summary statistics of key pollutants and meteorological parameters during the six case periods. As shown in Figure 4, PM_{2.5} usually started to increase at 6:00 a.m. and reached the highest level (even up to 333 µg/m³ in case 3) at 12:00–15:00 in the afternoon. Then, it gradually decreased and dropped to the lowest point at midnight. The average concentration of PM_{2.5} in mixed pollution episodes was 92.1 ± 32.1 µg/m³, exceeding the second grade of the Chinese National Ambient Air Quality Standard for daily average PM_{2.5} mass concentration (GB3095-2012, 75 µg/m³). The value was 2.12 times higher than that of the double low-level days. As for O₃, the average concentration remained at a high level, even reaching ~169.0 µg/m³ in case 6 (11–12 May 2016). As shown in Figure 4a, O₃ concentration was lower in the morning (6:00–8:00 a.m.) and evening (16:00–20:00 p.m.) but peaked in the afternoon (13:00–15:00 p.m.), which corresponded well to the traffic rushes and active photochemical period of one day. The morning (6:00–8:00 a.m.) and evening (16:00–20:00 p.m.) traffic rushes increased the concentrations of NO₂ and NO, and thus the lower O₃ concentrations at the two stages were mainly due to relatively weak solar radiation and NO titration. The O₃ concentration rapidly increased from 8:00 a.m. and reached the maximum value at 13:00–15:00 p.m., which was mainly due to the photolysis of accumulated NO₂ and the increasing active photochemical processes. Then, the O₃ was affected by vertical mixing, horizontal diffusion, and various physical and chemical consumptions in the atmosphere, and its concentration decreased until nighttime. The above results indicated that active photochemical reactions still occurred in the daytime under high PM_{2.5} concentration, in which the formation and accumulation of various oxidizing species including O₃ enhanced the conversions of NO₂ and SO₂ into NO₃⁻ and SO₄²⁻ and further promoted the evolution of fine particulate matter pollution.

In addition, O₃ concentration has a good correspondence with the temperature peak and RH trough. This is because that high temperature often means strong solar radiation. Moreover, O₃ diurnal variation between daytime and nighttime could be generally distinguished by solar radiation. Similar diurnal variation trends were also found in Malaysia [22]. It is noticeable that a rapid increase in PM_{2.5} mass concentration during these cases was often accompanied by the rapid rise of O₃ and kept for several hours in the daytime, and sometimes the two pollutants even peaked simultaneously. On the one hand, this result indicated that active photochemical processes still occurred and O₃ could be generated and accumulated under high-level PM_{2.5}. On the other hand, the occurrence of heavy fine particulate pollution can be closely associated with the active photochemical processes. The average mass concentration of O₃ was 151.7 ± 76.8 µg/m³ on the double high pollution days, which was 2.28 times higher than that of the double low days (66.5 ± 26.5 µg/m³). This result suggested strong atmospheric oxidizing capacity during the double high pollution cases, which would promote the formation of SIA and thus further enhance the concentration of PM_{2.5}. This study further confirmed that high fine particulate pollution and high ozone pollution can occur simultaneously under suitable atmospheric conditions.

Table 1. Summary of meteorological factors and chemical species data in the double high-level O₃ and PM_{2.5} pollution cases.

Parameter/Speciaies	Case 1	Case 2	Case 3	Case 4	Case 5	Case 6	Average
PM _{2.5} (µg/m ³)	93.7 ± 18.4	99.5 ± 39.3	95.2 ± 10.6	86.4 ± 34.6	97.4 ± 38.8	78.8 ± 25.9	92.1 ± 32.1
O ₃ (µg/m ³)	132.4 ± 63.6	122.9 ± 90.0	147.7 ± 104.3	143.8 ± 89.5	169.0 ± 57.1	155.8 ± 73.9	151.7 ± 76.8
O ₃ -8 h (µg/m ³)	145.4 ± 52.0	140.8 ± 74.5	169.7 ± 85.1	164.3 ± 73.6	174.1 ± 43.7	169.7 ± 54.6	146.8 ± 67.1
SO ₂ (µg/m ³)	23.25 ± 7.67	17.33 ± 10.69	26.92 ± 33.95	30.33 ± 4.71	20.36 ± 7.18	19.52 ± 6.02	22.15 ± 13.70
NO ₂ (µg/m ³)	36.50 ± 9.58	38.50 ± 11.99	53.54 ± 24.72	40.67 ± 10.03	35.78 ± 16.67	37.11 ± 19.00	39.04 ± 17.40
CO (µg/m ³)	789.17 ± 104.77	851.08 ± 233.43	948.00 ± 294.60	791.54 ± 106.86	1154.06 ± 386.35	993.81 ± 220.64	983.95 ± 312.48
NO _x (µg/m ³)	40.54 ± 11.92	45.17 ± 18.69	68.33 ± 52.56	46.54 ± 11.06	38.89 ± 18.53	48.21 ± 33.56	46.07 ± 28.32
K ⁺ (µg/m ³)	1.09 ± 0.13	1.58 ± 0.47	1.49 ± 0.25	1.06 ± 0.13	0.58 ± 0.29	0.47 ± 0.17	0.88 ± 0.49
Ca ²⁺ (µg/m ³)	0.24 ± 0.10	0.23 ± 0.14	0.22 ± 0.09	0.46 ± 0.07	0.25 ± 0.10	0.25 ± 0.09	0.27 ± 0.12
Na ⁺ (µg/m ³)	0.31 ± 0.04	0.35 ± 0.07	0.28 ± 0.04	0.32 ± 0.03	0.00 ± 0.00	0.22 ± 0.05	0.19 ± 0.14
Mg ²⁺ (µg/m ³)	0.09 ± 0.05	0.14 ± 0.05	0.11 ± 0.04	0.03 ± 0.04	0.06 ± 0.04	0.06 ± 0.03	0.08 ± 0.05
Cl ⁻ (µg/m ³)	1.02 ± 0.52	0.27 ± 0.49	0.00 ± 0.00	1.75 ± 0.40	0.98 ± 0.68	0.68 ± 0.44	0.81 ± 0.70
NO ₃ ⁻ (µg/m ³)	20.85 ± 7.68	20.72 ± 6.97	12.69 ± 5.74	13.45 ± 8.89	25.59 ± 14.31	17.53 ± 9.04	19.89 ± 11.43
SO ₄ ²⁻ (µg/m ³)	20.53 ± 5.53	27.18 ± 13.34	26.73 ± 5.05	22.30 ± 10.45	14.53 ± 4.59	14.98 ± 5.23	18.97 ± 8.71
NH ₄ ⁺ (µg/m ³)	12.97 ± 2.58	15.92 ± 5.84	12.98 ± 1.38	13.46 ± 5.86	13.91 ± 6.39	11.23 ± 4.44	13.27 ± 5.27
HONO (ppbv)	1.49 ± 0.55	2.18 ± 1.20	2.50 ± 1.49	4.74 ± 1.50	1.56 ± 0.79	2.14 ± 2.00	2.22 ± 1.64
HONO (ppbv) daytime	1.15 ± 0.38	2.00 ± 1.48	2.21 ± 1.78	4.21 ± 1.81	1.16 ± 0.75	1.48 ± 1.60	1.78 ± 1.60
SIA (µg/m ³)	54.35 ± 10.43	63.83 ± 24.19	52.40 ± 5.44	49.21 ± 21.65	54.03 ± 24.72	43.73 ± 17.09	52.13 ± 20.62
TWSI (µg/m ³)	57.09 ± 10.86	66.39 ± 25.08	54.50 ± 5.45	52.84 ± 21.78	55.91 ± 25.52	45.41 ± 17.58	54.36 ± 21.22
SIA/TWSI	0.95 ± 0.01	0.96 ± 0.01	0.96 ± 0.01	0.92 ± 0.03	0.97 ± 0.01	0.96 ± 0.01	0.96 ± 0.02
TWSI/PM _{2.5}	0.62 ± 0.10	0.68 ± 0.04	0.58 ± 0.07	0.61 ± 0.04	0.55 ± 0.11	0.56 ± 0.07	0.58 ± 0.09
SIA/PM _{2.5}	0.59 ± 0.09	0.65 ± 0.04	0.56 ± 0.07	0.56 ± 0.05	0.51 ± 0.13	0.54 ± 0.07	0.56 ± 0.08
NO ₃ ⁻ /SO ₄ ²⁻	1.13 ± 0.59	0.98 ± 0.53	0.52 ± 0.28	0.65 ± 0.42	1.64 ± 0.67	1.20 ± 0.68	1.17 ± 0.71
SOR	0.52 ± 0.09	0.68 ± 0.15	0.58 ± 0.09	0.82 ± 0.06	0.50 ± 0.11	0.65 ± 0.14	0.60 ± 0.15
NOR	0.30 ± 0.08	0.29 ± 0.09	0.16 ± 0.06	0.19 ± 0.10	0.34 ± 0.15	0.27 ± 0.13	0.28 ± 0.13
Temp (°C)	19.2 ± 4.8	21.4 ± 3.9	26.3 ± 3.8	29.6 ± 3.1	19.9 ± 3.8	20.9 ± 3.6	22.0 ± 5.1
RH (%)	72.2 ± 15.2	82.1 ± 13.4	65.7 ± 13.2	65.1 ± 11.6	53.2 ± 18.7	61.8 ± 12.9	63.6 ± 17.4
WS (m/s)	2.9 ± 1.2	2.7 ± 1.6	3.3 ± 1.4	1.0 ± 0.3	1.5 ± 0.6	1.6 ± 0.7	1.9 ± 1.2
Vis (km)	7.5 ± 2.7	5.1 ± 1.2	7.0 ± 1.5	10.1 ± 4.0	9.5 ± 7.2	9.0 ± 5.6	8.3 ± 5.3

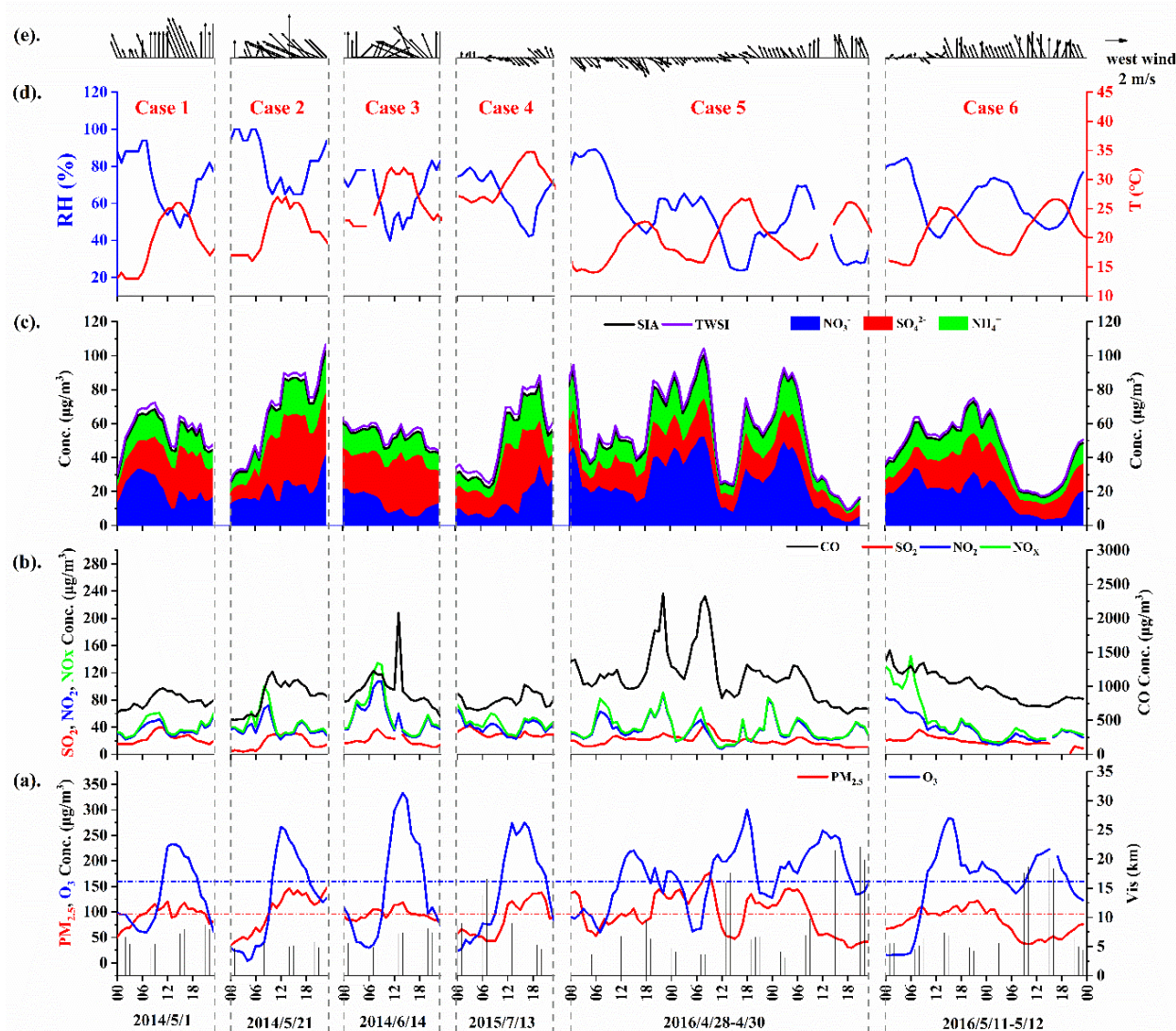


Figure 4. Time series of meteorological parameters and chemical species in double high-level O₃ and PM_{2.5} pollution cases. (a) PM_{2.5} (µg/m³), O₃ (µg/m³) and visibility (Vis, km); (b) SO₂, NO₂, NO_x and CO (µg/m³); (c) NO₃⁻, SO₄²⁻, NH₄⁺, SIA and TWSI (µg/m³); (d) temperature (T, °C) and relative humidity (RH, %); (e) wind direction and wind speed (m/s).

3.2.2. Characteristic of Water-Soluble Secondary Inorganic Ions in PM_{2.5} during the Double High-Level PM_{2.5} and O₃ Pollution Episodes

Chemical composition of fine particle matter is complex, including sulfate, nitrate, ammonium, organic carbon, inorganic carbon, and metal elements, among which secondary inorganic aerosol ions are important components [48,50]. In view of the high atmospheric oxidizing capacity during the double high pollution episodes, herein we mainly take SIA into consideration. In this study, the average mass concentration of SIA in PM_{2.5} was 52.13 ± 20.62 µg/m³ during the double high pollution episodes, which was about twice as much as that of the double low periods (Table 1 and Table S2). SIA accounted for 56% of the PM_{2.5} during the double high pollution episodes, which was higher than that in the previously reported haze events in Shanghai [48,50,51]. The value was also higher than those in some European countries where the ratios were 42–48% and $22.4\% \pm 16\%$ in Netherland and southern Italy, respectively [52,53]. This result indicated the high pollution characteristics of SIA and revealed that the secondary inorganic species were still one of the most predominant components of PM_{2.5} during the double high pollution periods.

Figure 4c indicated the mass concentrations of TWSI and SIA were intensely close in all cases, and their trends matched perfectly with $PM_{2.5}$. Both the TWSI and SIA had a good positive correlation with $PM_{2.5}$, for which the overall correlation coefficients (r) were 0.942 and 0.943, respectively. From Figure 4c, during the double high pollution cases, the hourly mass concentrations of $PM_{2.5}$ increased with a rapid rise of TWSI and SIA, which even showed the same peaks and troughs simultaneously. This result indicated that TWSI and SIA played a crucial role in the formation of $PM_{2.5}$, which is consistent with the previous studies [48].

The average mass concentrations of NH_4^+ , SO_4^{2-} , and NO_3^- were 13.27 ± 5.27 , 18.97 ± 8.71 , and $19.89 \pm 11.43 \mu\text{g}/\text{m}^3$ during the double high pollution cases (Table 1), respectively, which were 1.94, 2.60, and 1.66 times higher than those of the double low episodes (NH_4^+ : $6.83 \pm 4.44 \mu\text{g}/\text{m}^3$, SO_4^{2-} : $7.63 \pm 4.00 \mu\text{g}/\text{m}^3$, and NO_3^- : $11.97 \pm 9.58 \mu\text{g}/\text{m}^3$) (Table S2), respectively. This suggested the enhanced conversions of SO_2 and NO_2 and the enhanced formation of secondary SO_4^{2-} and NO_3^- [51], and then made a significant contribution to the high concentration of $PM_{2.5}$. The sulfur oxidation ratio (SOR) and the nitrate oxidation ratio (NOR) have usually been used as indicators of secondary transformation of gaseous species in the atmosphere [54], i.e., $SOR = n(SO_4^{2-}) / (n(SO_4^{2-}) + n(SO_2))$, $NOR = n(NO_3^-) / (n(NO_3^-) + n(NO_2))$ (n refers to the molar concentration). Meanwhile, as reported in previous studies, SOR values were less than 0.1 in primary emissions and higher than 0.1 when sulfate was produced through the secondary oxidation processes of SO_2 [55]. High SOR and NOR indicate that the secondary oxidation processes are obvious. The average values of SOR and NOR in the six double high pollution cases were 0.60 ± 0.15 and 0.28 ± 0.13 , respectively (Table 1), and the average values of SOR were generally higher than those of NOR. These values were higher than those observed in Shanghai in previous studies. For instance, Zhou et al. determined that the average values of SOR and NOR were 0.257 and 0.101 in 2011, respectively [56]. Hu et al. found that the average values of SOR and NOR on haze days in December 2013 were 0.32 ± 0.09 and 0.19 ± 0.13 , respectively [57]. Meanwhile, the SOR and NOR values in the double high pollution episodes were also higher than those in the double low cases, which were 0.48 ± 0.24 and 0.19 ± 0.10 for SOR and NOR, respectively (Table S2). Therefore, the high oxidation rates of SO_2 and NO_2 during the double high pollution episodes would lead to the formation of high levels of SO_4^{2-} and NO_3^- and thus led to further evolution of fine particulate pollution. The SOR value in Case 4 (Table 1, Figure S2) was 0.82 ± 0.06 , the highest value among all the cases. The T and RH in Case 4 were $29.6 \pm 3.1 \text{ }^\circ\text{C}$ and $65.1 \pm 11.6\%$, respectively, which were advantageous conditions for SO_2 to be transformed into SO_4^{2-} via a heterogeneous process [58]. Meanwhile, the relatively lower RH did not favor the interaction between O_3 and water molecules, but favored the accumulation of O_3 in Case 4, and therefore atmospheric oxidizing capacity was enhanced, which also accelerated the conversion of SO_2 to SO_4^{2-} . For NOR, in Case 1, 2, 5, and 6, NOR values were clearly higher than those in other cases. Relatively low T and/or relatively high RH were common features of Case 1, 2, 5, and 6, while low T and high RH favored a shift from the gas phase as nitric acid to the particulate phase as ammonium nitrate, which favored the formation of NO_3^- . Moreover, the temperatures in Case 3 and Case 4 were 26.3 ± 3.8 and $29.6 \pm 3.1 \text{ }^\circ\text{C}$, respectively, which were the higher temperatures in the six pollution cases, and hence the NOR values in these two cases were the lowest two values among all cases.

Figure 4c also showed the trends of individual secondary inorganic ions in the six pollution cases, from which we can find the different variations of SIA formation. On the whole, high temperature and high levels of SO_2 , O_3 , and NO_2 were favorable for the formation of SO_4^{2-} , whereas the impact of RH on the SO_4^{2-} formation was complex (Figure 4). The correlations of SO_4^{2-} concentration with RH were extremely highly negative in all the mixed pollution cases except Cases 5 and 6 ($r = 0.290$, -0.040 , respectively), with the highest value $r = 0.923$ ($p < 0.01$) in Case 4. The different correlation coefficients may suggest different formation pathways of atmospheric sulfate aerosols under different RH,

which led to different correlations between RH and SO_4^{2-} . High temperature not only promoted the reactions of SO_4^{2-} formation, but also often reflected strong solar radiation, and thus led to active atmospheric photochemistry, which further promoted the conversion of SO_2 and the formation of SO_4^{2-} [59]. The conspicuously positive correlations of SO_4^{2-} concentrations with temperature were found in all cases, among which the highest value was $r = 0.923$ ($p < 0.01$) in Case 4. Moreover, the high concentration of O_3 meant strong atmospheric oxidizing capacity, while the existence of high concentration of NO_2 might also promote the conversion of SO_2 [60], and thus all of these promoted the conversion of SO_2 and the formation of SO_4^{2-} . The effect of temperature and RH on nitrate formation was also complex. The correlation of NO_3^- with temperature was showing negative in Case 1, 3, 5, and 6 ($r = -0.512, -0.712, -0.625, \text{ and } -0.550$, respectively), while nonsignificant correlation showed in Case 2 ($r = 0.287$) and positive correlation in Case 4 ($r = 0.577$). For RH, positive correlations of NO_3^- with RH were found in Case 1, 3, 5, and 6 ($r = 0.560, 0.565, 0.447, \text{ and } 0.467$, respectively) and negative correlations in Case 4 ($r = -0.406$) and Case 2 ($r = -0.303$). The different correlation coefficients between NO_3^- and T or RH suggested the complex formation pathways of atmospheric nitrate aerosol under different T and RH. However, on the whole, the ambient condition of low temperature and high RH favored NO_3^- formation, which is consistent with a previous report [37]. To summarize, the concentrations of SO_4^{2-} and NO_3^- depended not only on the contents of their precursors such as SO_2 and NO_2 , but also on environmental conditions such as atmospheric oxidizing capacity, T and RH.

The mass ratio of $\text{NO}_3^-/\text{SO}_4^{2-}$ has been usually regarded as an indicator of the relative importance of mobile and stationary sources of sulfur and nitrogen in the atmosphere [37,61]. High $\text{NO}_3^-/\text{SO}_4^{2-}$ mass ratio means the predominance of mobile source over stationary source of pollutants [61]. The average value of $\text{NO}_3^-/\text{SO}_4^{2-}$ was 1.17 ± 0.71 in the six double high pollution cases. This result was close to that reported by Kong et al. (i.e., 1.00 during haze days in 2011) [48], but it also showed a marked difference from the other observations in Shanghai, for example, 0.67 in 2009 and 0.86 in 2012 [62]. Furthermore, the mass ratio value of our study was also higher than that of other megacities in China where average mass ratios were 1.02 in 2012 and 0.1–0.3 in 2006 in Beijing and Guangzhou, respectively [63]. The higher value in this study indicated that mobile vehicle emissions were making a significant contribution to $\text{PM}_{2.5}$ in Shanghai. This is consistent with the large vehicle population in Shanghai. In addition, Shanghai is not only located at the intersection of the East China Sea, but also on the waterway of the Yangtze River and Huangpu River, which included many mobile sources such as ship emissions. Therefore, the result showed the vital role of mobile sources in the double high pollution episodes in Shanghai. Besides industrial emissions, perhaps these sources emitted a lot of O_3 precursor NO_2 , making Shanghai urban area be a VOC-limited regime of O_3 formation.

3.2.3. Characteristic of Gaseous Pollutants and Meteorological Parameters during the Double High Pollution Episodes

Secondary sulfate and nitrate aerosols in the atmosphere are primarily originated from the conversions of SO_2 and NO_x released by anthropogenic sources. As shown in Figure 4b, the concentrations of SO_2 and NO_2 were affected by the morning and evening traffic rushes and the active photochemical processes. The enhancements of NO_2 concentrations were higher than those of SO_2 in most periods. The average mass concentrations of SO_2 and NO_2 during the whole double high pollution cases were 22.15 ± 13.70 and $39.04 \pm 17.40 \mu\text{g}/\text{m}^3$, respectively (Table 1). The average mass concentration of SO_2 was about 1.39 times higher than that in the double low periods ($17.11 \pm 8.67 \mu\text{g}/\text{m}^3$). However, the average NO_2 concentration in the double high cases was close to that in the double low cases ($38.67 \pm 21.96 \mu\text{g}/\text{m}^3$). For their specific changes, SO_2 was taken as an example. The concentration of SO_2 increased starting from 6:00 a.m. and reached a peak value at 8:00–9:00 a.m., and after 9:00 a.m., SO_2 concentration generally decreased until 14:00, and then it reached a secondary higher value of one day, which coincided with SO_4^{2-} formation. The rapid formation of sulfate during this period could be mainly attributed to SO_2

oxidation under active photochemical processes. The appearance of the secondary higher value is earlier than evening rush hours, suggesting that SO_2 was mainly emitted from stationary emissions rather than mobile emissions. From 9:00–16:00 the mass concentration of SO_4^{2-} increased continuously, suggesting that photochemical processes induced by solar radiation still played a significant role in SO_2 oxidation into SO_4^{2-} , though other oxidizing species such as NO_2 and O_3 may also play a role in SO_2 oxidation. After 16:00, both SO_2 and SO_4^{2-} showed decreasing trends. Noticeably, SO_2 concentration after 20:00 increased slightly, while no increasing trend of SO_4^{2-} was found, which confirmed the importance of sunlight in the formation processes of secondary sulfate aerosols.

Meanwhile, meteorological factors also played a key role in the formation processes of these secondary pollutants. The average RH and WS in the double high pollution cases were $63.6\% \pm 17.4\%$ and 1.9 ± 1.2 m/s (Table 1), and the wind speed in Figure 4e showed an overall calm condition. Wind speed less than 3 m/s could provide a stagnant atmospheric condition [64], which played a critical role in the formation and accumulation of O_3 and secondary species. The moderately high RH condition could enhance the hygroscopic growth of aerosol to form liquid droplets or water films on aerosol surfaces, and hence promote the heterogeneous processes for SIA formation [4,48]. As a result, moderately high RH and low WS together promoted the formation and accumulation of SIA and then further led to high concentration of $\text{PM}_{2.5}$.

Furthermore, Figure 5 showed the diurnal variations of surface boundary layer height (BLH) and solar radiation (SR) under the six double high pollution cases. Considering high $\text{PM}_{2.5}$ concentrations during the double high pollution periods, the SR could be lower than that during the double low periods due to light scattering of the high-level $\text{PM}_{2.5}$ [65]. Therefore, the high loading of fine particles would reduce O_3 concentration owing to its dimming effect [16]. However, O_3 concentration increased rapidly and immediately after $\text{PM}_{2.5}$ and then presented an overall simply unimodal at 13:00–15:00 throughout the whole day in the double high pollution cases. This result implied the photochemical formation of O_3 to some extent, though low solar radiation during the double high pollution cases rendered strong photochemical activity impossible. Combined with the changes of O_3 and $\text{PM}_{2.5}$ concentrations in Figure 4a, the daily variation trends of SR were consistent with those of O_3 and $\text{PM}_{2.5}$. This clearly indicated that there still existed active photochemical processes in the six double high pollution periods, which not only favored the formation of O_3 in the presence of high concentration $\text{PM}_{2.5}$, but also favored the enhancement of atmospheric oxidizing capacity and further promoted the formation of secondary aerosols and the increase of $\text{PM}_{2.5}$ concentrations. This was consistent with our previous discussion. Furthermore, as shown in Figure 5, BLH was always at a high level during the high solar radiation period of each day, and showed a change characteristic of first increasing and then decreasing, which was not only conducive to the enhanced formation of pollutants such as O_3 and $\text{PM}_{2.5}$ in the increasing period of BLH, but also conducive to the subsequent increase of O_3 and $\text{PM}_{2.5}$ concentrations in the decreasing period of BLH, promoting the formation and accumulation of secondary particulate pollutants in the atmospheric boundary level and resulting in serious mixed pollution episodes with high-levels of $\text{PM}_{2.5}$ and O_3 .

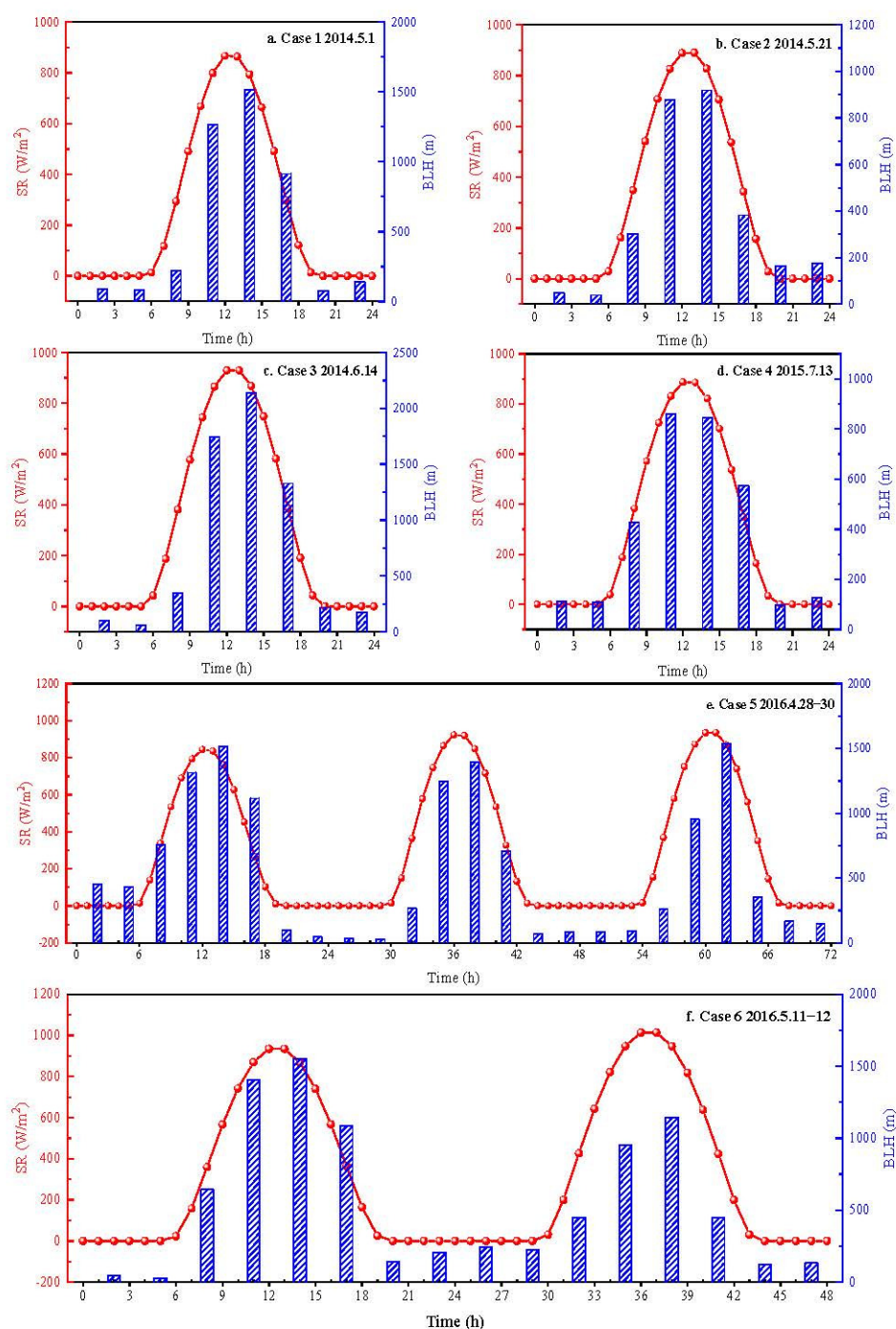


Figure 5. Variations of boundary layer height (BLH) and global solar radiation (SR) at ground level during the double high-level O₃ and PM_{2.5} pollution cases. (a) Case 1; (b) Case 2; (c) Case 3; (d) Case 4; (e) Case 5; (f) Case 6.

3.3. Formation Mechanisms of the Double High-Level O₃ and PM_{2.5} Episodes

To further understand the formation mechanisms of the double high-level O₃ and PM_{2.5} episodes, except for the correlations mentioned above, the correlations of O₃, PM_{2.5}, NO₂, NO, T, RH, and visibility (Vis) observed in each mixed pollution case were analyzed (Table S3). The correlations of PM_{2.5} with O₃ were positive in Case 2 (0.869), Case 3 (0.621), and Case 4 (0.828), and they were significant at the 0.01 level (two-tailed). These results not only suggested that a high concentration of O₃ could coexist with a high concentration of PM_{2.5}, but also implied that a high concentration of O₃ increased atmospheric oxidation, promoted the formation of secondary aerosols, and further increased the concentration

of $PM_{2.5}$. A strong positive correlation of temperature with O_3 was found in all the pollution cases, and the highest was 0.925 in Case 4. This result indicated that temperature could significantly affect the generation of O_3 , and this finding is similar to previous studies [22]. In contrast, RH presented a strong negative correlation with O_3 concentration. The highest correlation value was -0.919 in Case 4 ($RH \approx 65\%$). This result suggested that water molecules may destroy O_3 or the water film on particle surface or a droplet in the atmosphere may dissolve O_3 , and thus affect its production and accumulation, and therefore too high RH is not conducive to the formation and accumulation of gaseous O_3 , while moderate RH is conducive to the existence of high concentration of O_3 . In general, O_3 concentration has a strong positive correlation with temperature and solar radiation in summer [66], when it is usually with high visibility; meanwhile, under these circumstances, $PM_{2.5}$ concentration was often at a moderately low level. However, in this study, the correlations of $PM_{2.5}$ and visibility were negative in Cases 4–6 ($r = -0.800$, -0.812 , and -0.808 , respectively), and no correlation was found in Cases 1–3 ($r = -0.256$, 0.202 , and 0.113 , respectively). This result further suggested that $PM_{2.5}$ and O_3 could significantly affect the generation of each other. The negative correlations of $PM_{2.5}$ and RH were derived in all the pollution cases except Case 5 and 6, which may be due to the complex formation mechanism of secondary aerosols in $PM_{2.5}$ under different RH. For example, secondary sulfate aerosols in the atmosphere are usually formed through gas-phase oxidation at low RH, heterogeneous oxidation at moderate RH, and aqueous-phase oxidation at high RH [67]. The variations of RH in the six pollution episodes obviously increased the complexity of sulfate aerosol formation, and interfered with the correlation between $PM_{2.5}$ and RH. Meanwhile, the positive correlations between $PM_{2.5}$ and temperature were illustrated in all cases except Cases 5 and 6. Combining the results of $PM_{2.5}$ and O_3 with T and RH, we found that the conditions of high T and moderate RH was generally conducive to co-pollution of O_3 and $PM_{2.5}$. As for the important precursor of O_3 formation in photochemical reactions, NO_2 has moderate or weak negative correlations with O_3 in all cases. This may be due to the complex sources of NO_2 and the formation of some NO_2 via the oxidation of NO by O_3 . Negative correlations between O_3 and NO were found in all cases, which was mainly attributed to the titration effect of NO, which confirmed the oxidation reaction of NO by O_3 .

3.4. Impact of Daytime HONO on O_3 Formation during Double High-Level $PM_{2.5}$ and O_3 Pollution Cases

MARGA used pure water in WRD to absorb some trace gases, including HONO. The HONO measured by MARGA may be affected by the hydrolytic disproportionation of atmospheric NO_2 . However, NO_2 (g) is weakly dissolved in pure water (Henry's law constant $H \sim 0.01 \text{ M atm}^{-1}$), and its uptake coefficient on pure water is very small ($\gamma \sim 1 \times 10^{-7}$) [68]. Therefore, the formation of HONO from the dissolution of NO_2 (g) in pure water is unfavorable for both kinetic and thermodynamic reasons, and the influence of atmospheric NO_2 hydrolytic disproportionation on the measurement of HONO can be ignored. HONO data can be used to investigate the role of HONO in the formation of O_3 during the double high-level $PM_{2.5}$ and O_3 pollution episodes.

As mentioned in the introduction, several studies have reported that HONO photolysis was the dominant OH source. For example, HONO photolysis contributed 80.4% of atmospheric primary OH production in the wintertime [27], or more than 92% of atmospheric primary OH production in polluted areas [28]. Such a large contribution should greatly affect the formation of hydroperoxyl and organic peroxy radicals in the atmosphere, and then further significantly affect the formation of O_3 , and hence, the dominant contribution of HONO photolysis to primary OH production may increase the linear dependence between HONO and O_3 . Therefore, the relationships of daytime HONO and NO_2 with O_3 in each double high pollution case were analyzed to reveal the possible role of daytime HONO in O_3 formation.

Table 2 showed the correlation between O_3 and HONO (or NO_2) in each double high pollution case during the daytime. As shown in Table 2, negative correlations between

HONO (or NO₂) with O₃ were found during the daytime in all cases, indicating their consumption during the formation of O₃. For the relationship of HONO with O₃, there existed a strong negative correlation during 6:00–18:00 ($r = -0.860, -0.917, -0.918, -0.688, -0.811,$ and -0.769 for Cases 1–6, respectively). However, during the enhanced solar radiation period (8:00–16:00), the strong linear dependence between HONO and O₃ still existed in Cases 1–3 ($r = -0.871, -0.916,$ and $-0.935,$ respectively), Case 5 ($r = -0.900$), and Case 6 ($r = -0.676$), revealing the dominant role of HONO in O₃ formation during these pollution episodes. Meanwhile, this result may in turn suggest that HONO photolysis made a great contribution to atmospheric primary OH production during these pollution episodes. While the linear dependence between HONO and O₃ during the enhanced solar radiation periods (8:00–16:00) was weakened in Case 4 ($r = -0.385$). Case 4 had the highest average T (30.5 ± 3.0 °C), the lowest average WS (1.1 ± 0.3 m/s), and the highest average HONO (3.86 ± 0.99 µg/m³) and NH₃ (18.11 ± 1.03 µg/m³) concentrations, as well as the lower average NO₃[−] concentration (9.62 ± 4.47 µg/m³) during 8:00–16:00 among the six cases (Table S4). The high temperature was not conducive to the stability of ammonium nitrate, because the formed ammonium nitrate was thermodynamically unstable, which may elevate NH₃ concentration and decrease NO₃[−] concentration. Moreover, the observation of high HONO concentration at high temperature in Case 4 may imply the impacts of OH from other sources on the O₃ formation or the changes of HONO sources and O₃ formation pathways under the enhanced solar radiation. For example, OH radicals can also be produced by the photolysis of atmospheric nitrate aerosol, nitric acid, and H₂O₂ under solar radiation in the atmosphere [69,70], and the photolysis of atmospheric nitrate aerosol can also produce O(³P) [70], which may prompt the formation and accumulation of O₃. Additionally, the high average NH₃ concentration in Case 4 during the daytime may induce explosive growth in HONO by NH₃-promoted hydrolysis of NO₂ [71], which emerged as a relatively prominent HONO source compared to the other cases. All the mentioned above would disturb the linear dependence between daytime HONO and O₃ in Case 4. Meanwhile, it should be pointed out that the enhanced solar radiation in Case 4 could promote the photochemistry of NO₂ and thus enhance the negative correlation between NO₂ and O₃ (Table 2). In addition, compared to those in the double low cases (Table S5), there existed overall a stronger linear dependence between HONO and O₃ during the daytime (6:00–18:00) in all the cases except Case 4, revealing a more dominant role of HONO in O₃ formation and a more active atmospheric photochemical process during the double high pollution episodes. In short, the daytime HONO concentration was, on the whole, strongly negatively correlated with O₃ concentration during the double high pollution episodes, which not only revealed the dominant contribution of HONO photolysis to atmospheric primary OH production, but also indicated the indispensable role of HONO in O₃ formation during the double high pollution episodes.

Table 2. Correlation between O₃ and HONO (or NO₂) in each double high pollution case during daytime.

Double High Case		HONO		NO ₂	
		6:0–18:00	8:0–16:00	6:0–18:00	8:0–16:00
Case 1	O ₃	−0.860 **	−0.871 **	−0.822 **	−0.915 **
Case 2	O ₃	−0.917 **	−0.916 **	−0.658 **	−0.962 **
Case 3	O ₃	−0.918 **	−0.935 **	−0.825 **	−0.898 **
Case 4	O ₃	−0.688 **	−0.385	−0.208	−0.525
Case 5	O ₃	−0.811 **	−0.900 **	−0.683 **	−0.707 **
Case 6	O ₃	−0.769 **	−0.676 **	−0.602 **	−0.426

** with significant value at $p < 0.01$.

Compared to those in the double low cases during the daytime from 6:00 to 18:00 (Table S6), the average concentrations of HONO, O₃, SO₄^{2−}, NO₃[−], SIA, and PM_{2.5} on the double high pollution days were 1.18, 2.57, 2.62, 1.44, 1.90, and 2.12 times higher than those of the double low days (Table S4). The elevated O₃ on the double high pollution

days suggested the enhanced formation of O₃ and the enhanced atmospheric oxidizing capacity during the double high pollution cases, which would promote conversions of SO₂ and NO₂, and hence the enhanced formation of secondary SO₄²⁻, NO₃⁻, SIA, and PM_{2.5} was observed. However, it should be pointed out that the variable positive or negative correlations between daytime HONO and aerosol species (i.e., SO₄²⁻, NO₃⁻, SIA, and PM_{2.5}, Table S7) showed that the conversions of SO₂ and NO₂ were not entirely oxidized by HONO and its photolysis product OH, but they were likely to be oxidized by the other oxidizing species produced during the photochemical processes initiated by OH. Therefore, this result indicated the direct and indirect impacts of HONO on the formation of secondary species. Finally, K⁺ ion is the most commonly used tracer to judge and identify biomass burning pollution source [72], while biomass burning in agricultural activities can cause high PM_{2.5} and O₃ pollution in the YRD in China [17]. However, the low K⁺ concentration (0.88 ± 0.54 µg/m³, concentration range: 0.47 ± 0.17–1.58 ± 0.47 µg/m³) during the daytime in the double high pollution episodes excluded the impact of biomass burning events on O₃ formation [73].

4. Conclusions

This study focused on investigating the pollution characteristics and occurrence mechanisms of double high-level O₃ and PM_{2.5} pollution episodes and the significant role of daytime HONO in O₃ formation in these pollution episodes, based on almost-three-year observation measurements at the Pudong New Area environmental monitoring station in Shanghai. Results showed that high fine particulate pollution and high O₃ pollution could occur simultaneously. Even if the frequency of the occurrence of the double high pollution accounted for 1.0% in the whole observation period, the formation of PM_{2.5} and O₃ was intertwined and promoted mutually, which led to synchronous pollution both on long time scales and large regional scales and caused more serious air pollution. During the double high-level O₃ and PM_{2.5} pollution episodes there still existed active photochemical processes, while the active photochemical processes at high PM_{2.5} concentration favored the production and accumulation of O₃ under a calm atmospheric condition, including relatively high T, moderate RH, and low WS, which in turn enhanced the conversions of SO₂ and NO₂ and the formation and accumulation of secondary sulfate and nitrate aerosols, and further increased the concentration of PM_{2.5} and promoted the evolution of air pollution.

Furthermore, the daytime HONO concentration was, on the whole, strongly negatively correlated with O₃ concentration during the active photochemical processes of the double high pollution episodes, indicating that HONO plays a dominant role in the formation of O₃ in the double high pollution episodes. This result not only reveals the dominant contribution of HONO photolysis to the production of atmospheric OH and the indispensable role of HONO in O₃ formation during the double high pollution episodes, but also indicates the enhanced atmospheric oxidizing capacity by producing various oxidizing species for the oxidation of SO₂ and NO₂ during the double high pollution cases, which would promote the formation of SIA and further elevate the concentration of PM_{2.5}.

This study not only further confirmed that high fine particulate pollution and high O₃ pollution could occur simultaneously under suitable atmospheric conditions, but also highlighted the indispensable role of HONO in O₃ formation during the double high-level PM_{2.5} and O₃ pollution episodes, though HONO sources are still not well understood up to now, and therefore, it is very important to understand the additional HONO sources in the polluted air while collaborative control measures of O₃ and PM_{2.5} precursors have been carried out to improve the air quality in Shanghai and YRD region.

Supplementary Materials: The following are available online at <https://www.mdpi.com/article/10.3390/atmos12050557/s1>, Figure S1: Wind speed and directions at the observation site in December of 2014–2016, Figure S2: Variations of SOR, NOR, SO₂, NO₂, SO₄²⁻, NO₃⁻ in different double high-level O₃ and PM_{2.5} pollution cases, Table S1: Statistics of meteorological parameters during observation period 2014–2016, Table S2: Summary of meteorological factors and chemical species data in the

double low-level O₃ and PM_{2.5} pollution cases, Table S3: The correlation of ambient air pollutants and meteorological parameters in each double high-level pollution case, Table S4: Summary of meteorological factors and chemical species data in the double high-level O₃ and PM_{2.5} pollution cases during the daytime, Table S5: The correlation between O₃ and HONO (or NO₂) in each double low case during daytime, Table S6: Summary of the concentration data of HONO, O₃ and aerosol species in each double low case during the daytime, Table S7: The correlations between the daytime HONO and aerosol species (i.e., SO₄²⁻, NO₃⁻, SIA and PM_{2.5}) during the double high episodes.

Author Contributions: Conceptualization, L.K.; Investigation, K.Y., L.K. and F.S.; Validation, K.Y., L.K., J.S. and F.S.; Data curation, K.Y., S.J., L.K. and F.S.; Formal analysis, K.Y. and L.K.; Visualization, K.Y., S.T., L.C., C.W. and L.K.; Writing—original draft preparation, K.Y.; Writing—review and editing, K.Y., S.T., L.C., C.W., S.J., L.K. and L.W.; Funding acquisition, L.K. and L.W.; Project administration, L.K.; Supervision, L.K. All authors have read and agreed to the published version of the manuscript.

Funding: This research was funded by the National Natural Science Foundation of China (Grant Nos. 21777027, 21976032, and 41475110) and the National Key R & D Program of China (2017YFC0209505).

Institutional Review Board Statement: Not applicable.

Informed Consent Statement: Not applicable.

Data Availability Statement: The data reported in this study will be available on request from the corresponding author.

Conflicts of Interest: The authors declare that they have no conflict of interest.

References

1. Fu, Q.; Zhuang, G.; Wang, J.; Xu, C.; Huang, K.; Li, J.; Hou, B.; Lu, T.; Streets, D.G. Mechanism of formation of the heaviest pollution episode ever recorded in the Yangtze River Delta, China. *Atmos. Environ.* **2008**, *42*, 2023–2036. [[CrossRef](#)]
2. Chen, H.; Zhuang, B.; Liu, J.; Wang, T.; Li, S.; Xie, M.; Li, M.; Chen, P.; Zhao, M. Characteristics of ozone and particles in the near-surface atmosphere in the urban area of the Yangtze River Delta, China. *Atmos. Chem. Phys. Discuss.* **2019**, *19*, 4153–4175. [[CrossRef](#)]
3. Ding, X.; Kong, L.; Du, C.; Zhanzakova, A.; Fu, H.; Tang, X.; Wang, L.; Yang, X.; Chen, J.; Cheng, T. Characteristics of size-resolved atmospheric inorganic and carbonaceous aerosols in urban Shanghai. *Atmos. Environ.* **2017**, *167*, 625–641. [[CrossRef](#)]
4. Qiao, T.; Zhao, M.; Xiu, G.; Yu, J. Simultaneous monitoring and compositions analysis of PM₁ and PM_{2.5} in Shanghai: Implications for characterization of haze pollution and source apportionment. *Sci. Total. Environ.* **2016**, *557–558*, 386–394. [[CrossRef](#)] [[PubMed](#)]
5. Zhang, K.; Zhou, L.; Fu, Q.; Yan, L.; Morawska, L.; Jayaratne, R.; Xiu, G. Sources and vertical distribution of PM_{2.5} over Shanghai during the winter of 2017. *Sci. Total. Environ.* **2020**, *706*, 135683. [[CrossRef](#)]
6. Song, Y.; Tang, X.Y.; Fang, C.; Zhang, Y.H.; Hu, M.; Zeng, L.M.; Li, C.C.; Michael, B. Relationship between the visibility degradation and particle pollution in Beijing. *Acta Scien. Circum.* **2003**, *234*, 468–471.
7. Bell, M.L.; Davis, D.L.; Gouveia, N.; Borja-Aburto, V.H.; Cifuentes, L.A. The avoidable health effects of air pollution in three Latin American cities: Santiago, São Paulo, and Mexico City. *Environ. Res.* **2006**, *100*, 431–440. [[CrossRef](#)]
8. Seinfeld, J.H.; Pandis, S.N. *Atmospheric Chemistry and Physics: From Air Pollution to Climate Change*, 2nd ed.; John Wiley & Sons, Inc.: Hoboken, NJ, USA, 2006.
9. Huang, R.-J.; Zhang, Y.; Bozzetti, C.; Ho, K.-F.; Cao, J.-J.; Han, Y.; Daellenbach, K.R.; Slowik, J.G.; Platt, S.M.; Canonaco, F.; et al. High secondary aerosol contribution to particulate pollution during haze events in China. *Nat. Cell Biol.* **2014**, *514*, 218–222. [[CrossRef](#)] [[PubMed](#)]
10. Wang, T.; Xue, L.; Brimblecombe, P.; Lam, Y.F.; Li, L.; Zhang, L. Ozone pollution in China: A review of concentrations, meteorological influences, chemical precursors, and effects. *Sci. Total. Environ.* **2017**, *575*, 1582–1596. [[CrossRef](#)] [[PubMed](#)]
11. Abdullah, A.M.; Ismail, M.; Yuen, F.S.; Abdullah, S.; Elhadi, R.E. The relationship between daily maximum temperature and daily maximum ground level ozone concentration. *Pol. J. Environ. Stud.* **2017**, *26*, 517–523. [[CrossRef](#)]
12. Atkinson, R. Atmospheric chemistry of VOCs and NO_x. *Atmos. Environ.* **2000**, *34*, 2063–2101. [[CrossRef](#)]
13. Tong, L.; Zhang, H.; Yu, J.; He, M.; Xu, N.; Zhang, J.; Qian, F.; Feng, J.; Xiao, H. Characteristics of surface ozone and nitrogen oxides at urban, suburban and rural sites in Ningbo, China. *Atmos. Res.* **2017**, *187*, 57–68. [[CrossRef](#)]
14. Shen, X.; Sun, J.; Zhang, X.; Zhang, Y.; Zhang, L.; Che, H.; Ma, Q.; Yu, X.; Yue, Y. Characterization of submicron aerosols and effect on visibility during a severe haze-fog episode in Yangtze River Delta, China. *Atmos. Environ.* **2015**, *120*, 307–316. [[CrossRef](#)]
15. Zhang, Q.; Yan, R.; Fan, J.; Yu, S.; Yang, W.; Li, P.; Wang, S.; Chen, B.; Liu, W.; Zhang, X. A heavy haze episode in Shanghai in December of 2013: Characteristics, origins and implications. *Aerosol Air Qual. Res.* **2015**, *15*, 1881–1893. [[CrossRef](#)]
16. Zheng, G.J.; Duan, F.K.; Su, H.; Ma, Y.L.; Cheng, Y.F.; Zheng, B.; Zhang, Q.; Huang, T.; Kimoto, T.; Chang, D.; et al. Exploring the severe winter haze in Beijing: The impact of synoptic weather, regional transport and heterogeneous reactions. *Atmos. Chem. Phys. Discuss.* **2015**, *15*, 2969–2983. [[CrossRef](#)]

17. Ding, A.J.; Fu, C.B.; Yang, X.Q.; Sun, J.N.; Zheng, L.F.; Xie, Y.N.; Herrmann, E.; Nie, W.; Petäjä, T.; Kerminen, V.-M.; et al. Ozone and fine particle in the western Yangtze River Delta: An overview of 1 yr data at the SORPES station. *Atmos. Chem. Phys. Discuss.* **2013**, *13*, 5813–5830. [[CrossRef](#)]
18. Yue, D.; Zhong, L.; Zhang, T.; Shen, J.; Zhou, Y.; Zeng, L.; Dong, H.; Ye, S. Pollution properties of water-soluble secondary inorganic ions in atmospheric PM_{2.5} in the Pearl River Delta region. *Aerosol Air Qual. Res.* **2015**, *15*, 1737–1747. [[CrossRef](#)]
19. Zhang, G.; Xu, H.; Qi, B.; Du, R.; Gui, K.; Wang, H.; Jiang, W.; Liang, L.; Xu, W. Characterization of atmospheric trace gases and particulate matter in Hangzhou, China. *Atmos. Chem. Phys. Discuss.* **2018**, *18*, 1705–1728. [[CrossRef](#)]
20. Sun, W.; Wang, D.; Yao, L.; Fu, H.; Fu, Q.; Wang, H.; Li, Q.; Wang, L.; Yang, X.; Xian, A.; et al. Chemistry-triggered events of PM_{2.5} explosive growth during late autumn and winter in Shanghai, China. *Environ. Pollut.* **2019**, *254*, 112864. [[CrossRef](#)] [[PubMed](#)]
21. Li, L.; An, J.; Shi, Y.; Zhou, M.; Yan, R.; Huang, C.; Wang, H.; Lou, S.; Wang, Q.; Lu, Q.; et al. Source apportionment of surface ozone in the Yangtze River Delta, China in the summer of 2013. *Atmos. Environ.* **2016**, *144*, 194–207. [[CrossRef](#)]
22. Awang, N.R.; Ramli, N.A.; Shith, S.; Zainordin, N.S.; Manogaran, H. Transformational characteristics of ground-level ozone during high particulate events in urban area of Malaysia. *Air Qual. Atmos. Health* **2018**, *11*, 715–727. [[CrossRef](#)]
23. Tie, X.; Long, X.; Li, G.; Zhao, S.; Cao, J.; Xu, J. Ozone enhancement due to the photodissociation of nitrous acid in eastern China. *Atmos. Chem. Phys. Discuss.* **2019**, *19*, 11267–11278. [[CrossRef](#)]
24. Wang, D.; Zhou, B.; Fu, Q.; Zhao, Q.; Zhang, Q.; Chen, J.; Yang, X.; Duan, Y.; Li, J. Intense secondary aerosol formation due to strong atmospheric photochemical reactions in summer: Observations at a rural site in eastern Yangtze River Delta of China. *Sci. Total. Environ.* **2016**, *571*, 1454–1466. [[CrossRef](#)]
25. Li, K.; Jacob, D.J.; Shen, L.; Lu, X.; De Smedt, I.; Liao, H. Increases in surface ozone pollution in China from 2013 to 2019: Anthropogenic and meteorological influences. *Atmos. Chem. Phys.* **2020**, *20*, 11423–11433. [[CrossRef](#)]
26. Gao, J.; Li, Y.; Zhu, B.; Hu, B.; Wang, L.; Bao, F. What have we missed when studying the impact of aerosols on surface ozone via changing photolysis rates? *Atmos. Chem. Phys.* **2020**, *20*, 10831–10844. [[CrossRef](#)]
27. Kim, S.; VandenBoer, T.C.; Young, C.J.; Riedel, T.P.; Thornton, J.A.; Swarthout, B.; Sive, B.; Lerner, B.; Gilman, J.B.; Warneke, C.; et al. The primary and recycling sources of OH during the NACHTT-2011 campaign: HONO as an important OH primary source in the wintertime. *J. Geophys. Res. Atmos.* **2014**, *119*, 6886–6896. [[CrossRef](#)]
28. Xue, C.; Zhang, C.; Ye, C.; Liu, P.; Catoire, V.; Krysztofiak, G.; Chen, H.; Ren, Y.; Zhao, X.; Wang, J.; et al. HONO budget and its role in nitrate formation in the rural North China Plain. *Environ. Sci. Technol.* **2020**, *54*, 11048–11057. [[CrossRef](#)] [[PubMed](#)]
29. Liu, Z.; Wang, Y.; Gu, D.; Zhao, C.; Huey, L.G.; Stickel, R.; Liao, J.; Shao, M.; Zhu, T.; Zeng, L.; et al. Summertime photochemistry during CAREBeijing-2007: ROx budgets and O₃ formation. *Atmos. Chem. Phys.* **2012**, *12*, 7737–7752. [[CrossRef](#)]
30. Tang, Y.; An, J.; Wang, F.; Li, Y.; Qu, Y.; Chen, Y.; Lin, J. Impacts of an unknown daytime HONO source on the mixing ratio and budget of HONO, and hydroxyl, hydroperoxyl, and organic peroxy radicals, in the coastal regions of China. *Atmos. Chem. Phys. Discuss.* **2015**, *15*, 9381–9398. [[CrossRef](#)]
31. Aumont, B.; Chervier, F.; Laval, S. Contribution of HONO sources to the NO_x/HO_x/O₃ chemistry in the polluted boundary layer. *Atmos. Environ.* **2003**, *37*, 487–498. [[CrossRef](#)]
32. Li, Y.; An, J.; Min, M.; Zhang, W.; Wang, F.; Xie, P. Impacts of HONO sources on the air quality in Beijing, Tianjin and Hebei Province of China. *Atmos. Environ.* **2011**, *45*, 4735–4744. [[CrossRef](#)]
33. Du, H.; Kong, L.; Cheng, T.; Chen, J.; Yang, X.; Zhang, R.; Han, Z.; Yan, Z.; Ma, Y. Insights into Ammonium Particle-to-Gas Conversion: Non-sulfate Ammonium Coupling with Nitrate and Chloride. *Aerosol Air Qual. Res.* **2010**, *10*, 589–595. [[CrossRef](#)]
34. Makkonen, U.; Virkkula, A.; Mantykenttä, J.; Hakola, H.; Keronen, P.; Vakkari, V.; Aalto, P.P. Semi-continuous gas and inorganic aerosol measurements at a Finnish urban site: Comparisons with filters, nitrogen in aerosol and gas phases, and aerosol acidity. *Atmos. Chem. Phys.* **2012**, *12*, 5617–5631. [[CrossRef](#)]
35. Charron, A.; Harrison, R.M.; Moorcroft, S.; Booker, J. Quantitative interpretation of divergence between PM₁₀ and PM_{2.5} mass measurement by TEOM and gravimetric (Partisol) instruments. *Atmos. Environ.* **2004**, *38*, 415–423. [[CrossRef](#)]
36. Allen, G.; Sioutas, C.; Koutrakis, P.; Reiss, R.; Lurmann, F.W.; Roberts, P.T. Evaluation of the TEOM[®] method for measurement of ambient particulate mass in urban areas. *J. Air Waste Manag. Assoc.* **1997**, *47*, 682–689. [[CrossRef](#)] [[PubMed](#)]
37. Wang, T.; Wei, X.L.; Ding, A.J.; Poon, C.N.; Lam, K.S.; Li, Y.S.; Chan, L.Y.; Anson, M. Increasing surface ozone concentrations in the background atmosphere of Southern China, 1994–2007. *Atmos. Chem. Phys. Discuss.* **2009**, *9*, 6217–6227. [[CrossRef](#)]
38. Ding, A.; Wang, T.; Thouret, V.; Cammas, J.-P.; Nedelec, P. Tropospheric ozone climatology over Beijing: Analysis of aircraft data from the MOZAIC program. *Atmos. Chem. Phys. Discuss.* **2008**, *8*, 1–13. [[CrossRef](#)]
39. Lin, W.; Xu, X.; Zhang, X.; Tang, J. Contributions of pollutants from North China Plain to surface ozone at the Shangdianzi GAW Station. *Atmos. Chem. Phys.* **2008**, *8*, 5889–5898. [[CrossRef](#)]
40. Liu, N.W.; Lin, W.L.; Ma, J.Z.; Xu, W.Y.; Xu, X.B. Seasonal variation in surface ozone and its regional characteristics at global atmosphere watch stations in China. *J. Environ. Sci.* **2020**, *77*, 291–302. [[CrossRef](#)]
41. Xu, X.B.; Lin, W.L.; Xu, W.Y.; Jin, J.L.; Wang, Y.; Zhang, G.; Zhang, X.C.; Ma, Z.Q.; Dong, Y.Z.; Ma, Q.L.; et al. Long-term changes of regional ozone in China: Implications for human health and ecosystem impacts. *Elem. Sci. Anthrop.* **2020**, *8*, 13. [[CrossRef](#)]
42. Wang, T.; Cheung, V.T.F.; Anson, M.; Li, Y.S. Ozone and related gaseous pollutants in the boundary layer of eastern China: Overview of the recent measurements at a rural site. *Geophys. Res. Lett.* **2001**, *28*, 2373–2376. [[CrossRef](#)]
43. Zhao, M.F.; Huang, Z.S.; Qiao, T.; Zhang, Y.K.; Xiu, G.L.; Yu, J.Z. Chemical characterization, the transport pathways and potential sources of PM_{2.5} in Shanghai: Seasonal variations. *Atmos. Res.* **2015**, *158*, 66–78. [[CrossRef](#)]

44. Zhang, L.M.; Gong, S.L.; Padro, J.; Barrie, L. A size-segregated particle dry deposition scheme for an atmospheric aerosol module. *Atmos. Environ.* **2001**, *35*, 549–560. [[CrossRef](#)]
45. Khoder, M.I. Atmospheric conversion of sulfur dioxide to particulate sulfate and nitrogen dioxide to particulate nitrate and gaseous nitric acid in an urban area. *Chemosphere* **2002**, *49*, 675–684. [[CrossRef](#)]
46. Yu, S.C.; Zhang, Q.Y.; Yan, R.C.; Wang, S.; Li, P.F.; Chen, B.X.; Liu, W.P.; Zhang, X.Y. Origin of air pollution during a weekly heavy haze episode in Hangzhou, China. *Environ. Chem. Lett.* **2014**, *12*, 543–550. [[CrossRef](#)]
47. Huang, X.F.; Yu, J.Z.; Yuan, Z.; Lau, A.K.H.; Louie, P.K.K. Source analysis of high particulate matter days in Hong Kong. *Atmos. Environ.* **2009**, *43*, 1196–1203. [[CrossRef](#)]
48. Kong, L.D.; Du, C.T.; Zhanzakova, A.; Cheng, T.T.; Yang, X.; Wang, L.; Fu, H.B.; Chen, J.M.; Zhang, S.C. Trends in heterogeneous aqueous reaction in continuous haze episodes in suburban Shanghai: An in-depth case study. *Sci. Total Environ.* **2018**, *634*, 1192–1204. [[CrossRef](#)] [[PubMed](#)]
49. Ming, L.L.; Jin, L.; Li, J.; Fu, P.Q.; Yang, W.Y.; Liu, D.; Zhang, G.; Wang, Z.F.; Li, X.D. PM_{2.5} in the Yangtze River Delta, China: Chemical compositions, seasonal variations, and regional pollution events. *Environ. Pollut.* **2017**, *223*, 200–212. [[CrossRef](#)] [[PubMed](#)]
50. Du, H.H.; Kong, L.D.; Cheng, T.T.; Chen, J.M.; Du, J.F.; Li, L.; Xia, X.G.; Leng, C.P.; Huang, G.H. Insights into summertime haze pollution events over Shanghai based on online water-soluble ionic composition of aerosols. *Atmos. Environ.* **2011**, *45*, 5131–5137. [[CrossRef](#)]
51. Wang, H.L.; Qiao, L.P.; Lou, S.R.; Zhou, M.; Chen, J.M.; Wang, Q.; Tao, S.K.; Chen, C.H.; Huang, H.Y.; Li, L.; et al. PM_{2.5} pollution episode and its contributors from 2011 to 2013 in urban Shanghai, China. *Atmos. Environ.* **2015**, *123*, 298–305. [[CrossRef](#)]
52. Cesari, D.; De Benedetto, G.E.; Bonasoni, P.; Busetto, M.; Dinoi, A.; Merico, E.; Chirizzi, D.; Cristofanelli, P.; Donato, A.; Grasso, F.M.; et al. Seasonal variability of PM_{2.5} and PM₁₀ composition and sources in an urban background site in Southern Italy. *Sci. Total Environ.* **2018**, *612*, 202–213. [[CrossRef](#)]
53. Mooibroek, D.; Schaap, M.; Weijers, E.P.; Hoogerbrugge, R. Source apportionment and spatial variability of PM_{2.5} using measurements at five sites in the Netherlands. *Atmos. Environ.* **2011**, *45*, 4180–4191. [[CrossRef](#)]
54. Sun, Y.L.; Zhuang, G.S.; Tang, A.H.; Wang, Y.; An, Z.S. Chemical characteristics of PM_{2.5} and PM₁₀ in haze-fog episodes in Beijing. *Environ. Sci. Technol.* **2006**, *40*, 3148–3155. [[CrossRef](#)] [[PubMed](#)]
55. Ohta, S.; Okita, T. A chemical characterization of atmospheric aerosol in Sapporo. *Atmos. Environ.* **1990**, *24*, 815–822. [[CrossRef](#)]
56. Zhou, M.; Qiao, L.P.; Zhu, S.H.; Li, L.; Lou, S.R.; Wang, H.L.; Wang, Q.; Tao, S.K.; Huang, C.; Chen, C.H. Chemical characteristics of fine particles and their impact on visibility impairment in Shanghai based on a 1-year period observation. *J. Environ. Sci.* **2016**, *48*, 151–160. [[CrossRef](#)] [[PubMed](#)]
57. Hu, Q.Q.; Fu, H.B.; Wang, Z.Z.; Kong, L.D.; Chen, M.D.; Chen, J.M. The variation of characteristics of individual particles during the haze evolution in the urban Shanghai atmosphere. *Atmos. Res.* **2016**, *18*, 95–105. [[CrossRef](#)]
58. Zhao, Y.; Liu, Y.C.; Ma, J.Z.; Ma, Q.X.; He, H. Heterogeneous reaction of SO₂ with soot: The roles of relative humidity and surface composition of soot in surface sulfate formation. *Atmos. Environ.* **2017**, *152*, 465–476. [[CrossRef](#)]
59. Leng, C.P.; Duan, J.Y.; Xu, C.; Zhang, H.F.; Wang, Y.F.; Wang, Y.Y.; Li, X.; Kong, L.D.; Tao, J.; Zhang, R.J.; et al. Insights into a historic severe haze event in Shanghai: Synoptic situation, boundary layer and pollutants. *Atmos. Chem. Phys.* **2016**, *16*, 9221–9234. [[CrossRef](#)]
60. He, H.; Wang, Y.S.; Ma, Q.X.; Ma, J.Z.; Chu, B.W.; Ji, D.S.; Tang, G.Q.; Liu, C.; Zhang, H.X.; Hao, J.M. Mineral dust and NO_x promote the conversion of SO₂ to sulfate in heavy pollution days. *Sci. Rep.* **2014**, *4*, 4172. [[CrossRef](#)]
61. Arimoto, R.; Duce, R.A.; Savoie, D.L.; Prospero, J.M.; Talbot, R.; Cullen, J.D.; Tomza, U.; Lewis, N.F.; Jay, B.J. Relationships among aerosol constituents from Asia and the North Pacific during PEM-West A. *J. Geophys. Res. Atmos.* **1996**, *101*, 2011–2023. [[CrossRef](#)]
62. Zhao, M.F.; Qiao, T.; Huang, Z.S.; Zhu, M.Y.; Xu, W.; Xiu, G.L.; Tao, J.; Lee, S.C. Comparison of ionic and carbonaceous compositions of PM_{2.5} in 2009 and 2012 in Shanghai, China. *Sci. Total Environ.* **2015**, *536*, 695–703. [[CrossRef](#)] [[PubMed](#)]
63. Han, T.T.; Liu, X.G.; Zhang, Y.H.; Gu, J.W.; Tian, H.Z.; Zeng, L.M.; Chang, S.Y.; Cheng, Y.F.; Lu, K.D.; Hu, M. Chemical characteristics of PM₁₀ during the summer in the mega-city Guangzhou, China. *Atmos. Res.* **2014**, *137*, 25–34. [[CrossRef](#)]
64. Ghazali, N.A.; Ramli, N.A.; Yahaya, A.S.; Yusof, N.F.F.M.D.; Sansuddin, N.; Al Madhoun, W.A. Transformation of nitrogen dioxide into ozone and prediction of ozone concentrations using multiple linear regression techniques. *Environ. Monit. Assess.* **2010**, *165*, 475–489. [[CrossRef](#)]
65. David, Y.H.; Sheng, C.; Chen, S.C.; Zou, Z. PM_{2.5} in China: Measurements, sources, visibility and health effects, and mitigation. *Particuology* **2014**, *13*, 1–26.
66. Pudasainee, D.; Sapkota, B.; Shrestha, M.L.; Kaga, A.; Kondo, A.; Inoue, Y. Ground level ozone concentrations and its association with NO_x and meteorological parameters in Kathmandu valley, Nepal. *Atmos. Environ.* **2006**, *40*, 8081–8087. [[CrossRef](#)]
67. Shen, X.H.; Lee, T.Y.; Guo, J.; Wang, X.F.; Li, P.H.; Xu, P.J.; Wang, Y.; Ren, Y.; Wang, W.; Wang, T.; et al. Aqueous phase sulfate production in clouds in eastern China. *Atmos. Environ.* **2012**, *62*, 502–511. [[CrossRef](#)]
68. Lee, Y.N.; Schwartz, S.E. Reaction kinetics of nitrogen dioxide with liquid water at low partial pressure. *J. Phys. Chem.* **1981**, *85*, 840–848. [[CrossRef](#)]
69. Schiffman, A.; Nelson, D.D., Jr.; Nesbitt, D.J. Quantum yields for OH production from 193 and 248 nm photolysis of HNO₃ and H₂O₂. *J. Chem. Phys.* **1993**, *98*, 6935–6946. [[CrossRef](#)]

70. Schuttlefield, J.; Rubasinghege, G.; El-Maazawi, M.; Bone, J.; Grassian, V.H. Photochemistry of adsorbed nitrate. *J. Am. Chem. Soc.* **2008**, *130*, 12210–12211. [[CrossRef](#)]
71. Xu, W.; Kuang, Y.; Zhao, C.; Tao, J.; Zhao, G.; Bian, Y.; Yang, W.; Yu, Y.; Shen, C.; Liang, L.; et al. NH₃-promoted hydrolysis of NO₂ induces explosive growth in HONO. *Atmos. Chem. Phys.* **2019**, *19*, 10557–10570. [[CrossRef](#)]
72. Li, J.; Posfai, M.; Hobbs, P.V.; Buseck, P.R. Individual aerosol particles from biomass burning in southern Africa: 2. compositions and aging of inorganic particles. *J. Geophys. Res. Atmos.* **2003**, *108*, 8484. [[CrossRef](#)]
73. Tong, S.Y.; Kong, L.D.; Yang, K.J.; Shen, J.D.; Chen, L.; Jin, S.Y.; Wang, C.; Sha, F.; Wang, L. Characteristics of air pollution episodes influenced by biomass burning pollution in Shanghai, China. *Atmos. Environ.* **2020**, *238*, 117756. [[CrossRef](#)]